Monthly Notices of the ROYAL ASTRONOMICAL SOCIETY

MNRAS **521,** 5046–5063 (2023) https://doi.org/10.1093/mnras/stad767
Advance Access publication 2023 March 20

Neutrino follow-up with the Zwicky transient facility: results from the first 24 campaigns

Robert Stein [1,2,3★] Simeon Reusch [1,2] Anna Franckowiak [1,2,4] Marek Kowalski [1,2] Jannis Necker [1,2] Sven Weimann,[4] Mansi M. Kasliwal [3] Jesper Sollerman [5] Tomas Ahumada [6,7] Pau Amaro Seoane [8,9,10] Shreya Anand [3] Igor Andreoni [11,12,13] Eric C. Bellm [14] Joshua S. Bloom [15,16] Michael Coughlin [17] Kishalay De,[18] Christoffer Fremling [3] Suvi Gezari [19] Matthew Graham [3] Steven L. Groom [20] George Helou [20] David L. Kaplan [21] Viraj Karambelkar [3] Albert K.H. Kong [22] Erik C. Kool [5] Massimiliano Lincetto [4] Ashish A. Mahabal [3,23] Frank J. Masci [20] Michael S. Medford [15,16] Robert Morgan [24] Jakob Nordin [2] Hector Rodriguez,[25] Yashvi Sharma [3] Jakob van Santen [1] Sjoert van Velzen [26] and Lin Yan [25]

Affiliations are listed at the end of the paper

Accepted 2023 March 5. Received 2023 February 25; in original form 2022 April 8

ABSTRACT

The Zwicky Transient Facility (ZTF) performs a systematic neutrino follow-up programme, searching for optical counterparts to high-energy neutrinos with dedicated Target-of-Opportunity (ToO) observations. Since first light in March 2018, ZTF has taken prompt observations for 24 high-quality neutrino alerts from the IceCube Neutrino Observatory, with a median latency of 12.2 h from initial neutrino detection. From two of these campaigns, we have already reported tidal disruption event (TDE) AT 2019dsg and likely TDE AT 2019fdr as probable counterparts, suggesting that TDEs contribute >7.8 per cent of the astrophysical neutrino flux. We here present the full results of our programme through to December 2021. No additional candidate neutrino sources were identified by our programme, allowing us to place the first constraints on the underlying optical luminosity function of astrophysical neutrino sources. Transients with optical absolutes magnitudes brighter that −21 can contribute no more than 87 per cent of the total, while transients brighter than −22 can contribute no more than 58 per cent of the total, neglecting the effect of extinction and assuming they follow the star formation rate. These are the first observational constraints on the neutrino emission of bright populations such as superluminous supernovae. None of the neutrinos were coincident with bright optical AGN flares comparable to that observed for TXS 0506+056/IC170922A, with such optical blazar flares producing no more than 26 per cent of the total neutrino flux. We highlight the outlook for electromagnetic neutrino follow-up programmes, including the expected potential for the Rubin Observatory.

Key words: neutrinos – astroparticle physics – transients: tidal disruption events – transients: supernovae – gamma-ray bursts..

1 INTRODUCTION

Astrophysical neutrinos are produced through the interaction of accelerated hadrons with matter or photons. A flux of astrophysical neutrinos with energies in the TeV–PeV range, was first discovered by IceCube in 2013 (IceCube Collaboration 2013). Recent results suggest that a substantial fraction of these high-energy neutrinos are produced in the cores of Active Galactic Nuclei (AGN) (Abbasi et al. 2022), with additional evidence for neutrino emission from the nearby AGN NGC 1068 (Aartsen et al. 2020). Beyond this static component, various transient or variable source classes have been proposed as possible contributors to the neutrino flux, including gamma-ray bursts (GRBs) (Waxman & Bahcall 1997), core-collapse supernovae (CCSNe) (Murase et al. 2011), TDEs (Farrar & Gruzinov 2009), and blazars (Mannheim 1993). All of these proposed neutrino source classes have electromagnetic signatures at optical wavelengths.

To aid in identifying these time-varying source candidates, IceCube has operated an automated programme since 2016 to publish realtime high-energy neutrino alerts (Aartsen et al. 2017), enabling contemporaneous electromagnetic observations of putative neutrino source candidates at radio (Kadler et al. 2021), optical (Kowalski & Mohr 2007; Aartsen et al. 2015; Morgan et al. 2019; Pan-Starrs Collaboration et al. 2019; Necker et al. 2022), X-ray (Evans et al. 2015; Ferrigno et al. 2021), and gamma-ray wavelengths (Lucarelli et al. 2019; Garrappa et al. 2021; Satalecka et al. 2021). In 2017, this realtime programme led to the identification of a flaring blazar, TXS 0506+056, as the likely source of high-energy neutrino IC170922A (IceCube Collaboration et al. 2018). Studies of these high-energy

★ E-mail: rdstein@caltech.edu

neutrino alerts have suggested possible correlations with blazar subpopulations, namely radio-bright blazars (Plavin et al. 2020, 2021) and intermediate-energy/high-energy peaked blazars (IBLs/HBLs) (Giommi et al. 2020a).

The Zwicky Transient Facility (ZTF) is an optical telescope with a 47 sq. deg field of view (Bellm et al. 2019a; Dekany et al. 2020). Since first light in 2018, ZTF has operated a dedicated neutrino follow-up programme, in which the arrival directions of IceCube neutrino alerts are observed with Target-of-Opportunity (ToO) observations (Graham et al. 2019). This programme has led to the identification of two further likely high-energy neutrino sources, the TDE AT 2019dsg (Stein et al. 2021b) and the probable TDE AT 2019fdr (Reusch et al. 2022, though see Pitik et al. 2022 for an alternative interpretation). Accounting for the contribution of higher-redshift sources, these results suggest that at least 7.8 per cent of neutrino alerts arise from the broader TDE population (Reusch et al. 2022). Archival analysis of ZTF data revealed further evidence of a correlation between such flares and high-energy neutrinos (van Velzen et al. 2021).

In this paper we outline the full results of the ZTF neutrino follow-up programme, which has to date included 24 dedicated neutrino follow-up campaigns. This sample enables novel constraints to be set on the neutrino emission of a broad range of optical transient and variable populations.

The paper is organized as follows: Section 2outlines the programme itself, including trigger criteria and optical candidate selection. Section 3outlines transient candidates identified by the programme, and subsequent electromagnetic observations to determine their nature. Section 4 outlines optical AGN flares found coincident with neutrinos, and Section 5 provides data on two candidate neutrino sources identified in the literature. Section 6 considers the various constraints that can be placed on different possible neutrino source populations from our programme. Section 7summarizes the main results, and outlines how such follow-up programmes may improve with future observatories.

2 NEUTRINO FOLLOW-UP WITH ZTF

Neutrino alerts are generally published by IceCube in the form of automated Gamma-ray Coordination Network (GCN) Notices[1], with initial estimates of the statistical uncertainty on the neutrino position. These positions are then superseded after a few hours by a GCN Circular with an updated localization that also incorporates systematic uncertainties (Lagunas Gualda et al. 2021). Given the substantial increase in localization area once systematic effects are accounted for, with increases of factor 5 not being uncommon, we rely on the latter category to perform our search for neutrino counterparts.

With ZTF, we aim to observe all accessible high-quality neutrino alerts from IceCube. We define high-quality alerts as those with a high probability to be of astrophysical origin ('signalness' $>$ 50 per cent), or those which are well-localized (a 90 per cent localization area $<$ 10 sq. deg.). Though IceCube labels alerts as Gold or Bronze based on average quality, individual Bronze alerts have been reported with signalness values greater than 50 per cent (e.g. IC211208A) and Gold alerts have been reported with signalness values less than 15 per cent (e.g. IC201130A). We therefore ignore the labelling of these streams, and select exclusively based on the signalness and localization.

We have followed up 24 neutrinos in the period from survey start on 2018 March 20 – 2021 December 31, out of a total of 79 neutrino alerts published by IceCube during that time. Table 1 summarizes each neutrino alert observed by ZTF. From 2019 June 17, IceCube published neutrino alerts with improved selection criteria (V2) to provide an elevated alert rate (Blaufuss et al. 2019). In addition to 1 of the 12 alerts under the old selection, ZTF followed up 23 of the 67 alerts published under the V2 selection. Mid-way through the ZTF programme, an additional cut on neutrino alert galactic latitude ($|b| > 10$ deg) was introduced to avoid crowded fields with many stars.

Each neutrino localization region can typically be covered by one or two observations of fields in a predefined ZTF 'grid' tiling of the sky. Multiple observations are scheduled for each field, with both g and r filters, and a separation of at least 15 min between images. These observations typically last for 300 s, with a typical limiting magnitude of 21.5. ToO observations are typically conducted on the first two nights following a neutrino alert, before swapping to serendipitous coverage with shorter 30 s exposures and a 2-d cadence as part of the public survey (Bellm et al. 2019b). As can be seen in Fig. 1, our first coverage of events has a median latency of 12.2 h from neutrino detection. Some latency is unavoidable because the neutrino localization itself is typically only released with a delay of $\gtrsim$2 h, but additional latency arises primarily due to observability constraints. Poor weather can prevent observations on the first night after neutrino detection, leading to 20 per cent of alerts observed with a latency $>$24 h. Serendipitous coverage from the public survey, with a median latency of 24 h after neutrino detection, reduces the latency for some campaigns.

As for all ZTF data, these observations are first processed by the Infra-red Processing and Analysis Centre (IPAC) to identify detections in difference images (Masci et al. 2019). These detections are then packaged as 'alerts' (Patterson et al. 2019), and processed by our dedicated data analysis pipeline, *NuZTF* (Stein, Reusch & Necker 2021a), which searches for extragalactic ZTF detections coincident with external triggers. For neutrinos followed-up by ZTF, we define spatial coincidence as requiring that an object lies within the reported 90 per cent localization rectangle from IceCube, and define temporal coincidence as requiring that an object is detected at least once following the neutrino arrival time.

NuZTF is built using the *AMPEL* software framework (Nordin et al. 2019), based on a search algorithm for extragalactic transients. Cuts are applied to reject spurious detections, stars and solar system objects (see Stein et al. 2021b for more details). Searching for detections in the window from neutrino arrival time to 14 d post-neutrino, these cuts typically yield 1 good candidate per $\sim$3 sq. deg. of observed sky.

Promising candidates are prioritized for spectroscopic classification, to confirm or rule out a possible association with a given neutrino. Once classified, an object can then be cross-referenced to relevant neutrino emission scenarios for that population. In particular, optical signatures we look for include:

(i) **Supernovae with evidence of CSM interaction**. High-energy neutrinos are thought to be produced when CCSNe occur within a dense circumstellar medium (CSM), with the resultant shock collisions then generating neutrino emission simultaneously with the optical light curve (Murase et al. 2011). The presence of such CSM interaction also results in characteristic narrow lines in the optical spectrum, so these models generally apply to the Type IIn supernova population which exhibits these lines. The neutrino emission is expected to be highest close to optical peak, and to then decay over time. In this case, the expected optical signature would be any supernova with evidence of ongoing CSM interaction.

[1] https://gcn.gsfc.nasa.gov

Table 1. Summary of the 24 neutrino alerts followed up by ZTF since survey start on 2018 March 20.

Event	R.A. (J2000) [deg]	Dec (J2000) [deg]	90 per cent area [sq. deg.]	ZTF obs [sq. deg.]	Latency [hours]	Signalness	References
IC190503A	120.28	+ 6.35	1.9	1.4	10.2	36 per cent	Blaufuss (2019c) Stein et al. (2019a)
IC190619A	343.26	+ 10.73	27.2	21.6	20.9	55 per cent	Blaufuss (2019e) Stein et al. (2019b)
IC190730A	225.79	+ 10.47	5.4	4.5	7.5	67 per cent	Stein (2019a) Stein et al. (2019c)
IC190922B	5.76	−1.57	4.5	4.1	8.0	51 per cent	Blaufuss (2019h) Stein et al. (2019d)
IC191001A	314.08	+ 12.94	25.5	23.1	7.4	59 per cent	Stein (2019c) Stein et al. (2019e)
IC200107A	148.18	+ 35.46	7.6	6.3	2.0	–	Stein (2020a) Stein & Reusch (2020)
IC200109A	164.49	+ 11.87	22.5	22.4	32.4	77 per cent	Stein (2020b) Reusch & Stein (2020a)
IC200117A	116.24	+ 29.14	2.9	2.7	22.0	38 per cent	Lagunas Gualda (2020a) Reusch & Stein (2020b) Reusch & Stein (2020c)
IC200512A	295.18	+ 15.79	9.8	9.3	1.7	32 per cent	Lagunas Gualda (2020c) Reusch, Stein & Franckowiak (2020a)
IC200530A	255.37	+ 26.61	25.3	22.0	0.2	59 per cent	Stein (2020e) Reusch et al. (2020b) Reusch et al. (2020c)
IC200620A	162.11	+ 11.95	1.7	1.2	25.8	32 per cent	Santander (2020b) Reusch, Stein & Franckowiack (2020e)
IC200916A	109.78	+ 14.36	4.2	3.6	14.7	32 per cent	Blaufuss (2020e) Reusch et al. (2020f) Reusch et al. (2020g)
IC200926A	96.46	−4.33	1.7	1.3	4.1	44 per cent	Lagunas Gualda (2020g) Reusch et al. (2020h)
IC200929A	29.53	+ 3.47	1.1	0.9	14.1	47 per cent	Lagunas Gualda (2020h) Weimann et al. (2020a)
IC201007A	265.17	+ 5.34	0.6	0.6	4.8	88 per cent	Santander (2020c) Reusch et al. (2020i)
IC201021A	260.82	+ 14.55	6.9	6.3	43.7	30 per cent	Lagunas Gualda (2020i) Stein et al. (2020b)
IC201130A	30.54	−12.10	5.4	4.5	7.1	15 per cent	Lagunas Gualda (2020l) Weimann et al. (2020b)
IC201209A	6.86	−9.25	4.7	3.2	16.9	19 per cent	Lagunas Gualda (2020m) Reusch et al. (2020j)
IC201222A	206.37	+ 13.44	1.5	1.4	35.2	53 per cent	Blaufuss (2020k) Stein et al. (2020c)
IC210210A	206.06	+ 4.78	2.8	2.1	0.2	65 per cent	Lagunas Gualda (2021a) Reusch et al. (2021)
IC210510A	268.42	+ 3.81	4.0	3.7	5.1	28 per cent	Santander (2021c) Stein et al. (2021c)
IC210629A	340.75	+ 12.94	6.0	4.6	15.4	35 per cent	Santander (2021f) Necker et al. (2021)
IC210811A	270.79	+ 25.28	3.2	2.7	26.7	66 per cent	Santander (2021h) Stein et al. (2021d)
IC210922A	60.73	−4.18	1.6	1.2	16.1	92 per cent	Lincetto (2021a) Weimann et al. (2021)

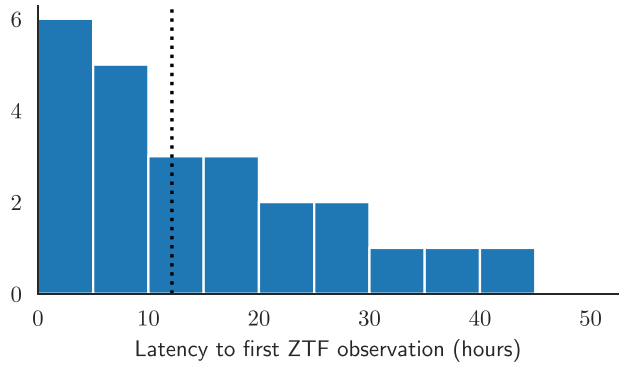

Figure 1. Latency between neutrino detection and first ZTF coverage. The median latency time of 12.2 h is indicated by the vertical dotted line.

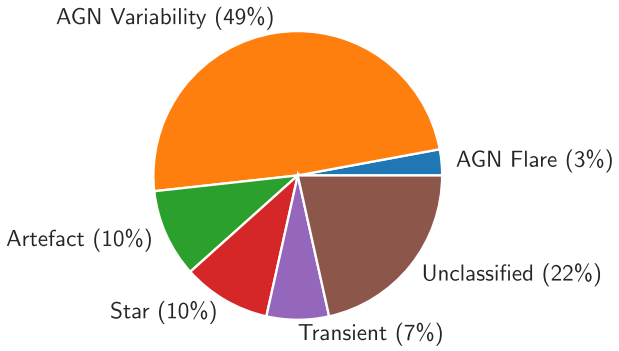

Figure 2. Breakdown of the classification of 172 candidates selected by our programme for visual inspection.

(ii) **Supernovae with relativistic jets**. Some supernovae have been observed to launch relativistic jets as part of the core-collapse process (Galama et al. 1998). Those jets which proceed to escape the surrounding stellar envelope and CSM can be observed as long GRBs if they are oriented towards Earth. Analogously, where an on-axis supernova jet does not escape the stellar envelope, there would instead be a so-called 'choked jet' (Nakar 2015). For both scenarios, neutrino emission would primarily be expected during the 'prompt phase', in the ∼100 s after supernova explosion (Waxman & Bahcall 1997; Senno, Murase & Mészáros 2016). This scenario would then lead to a young supernova, typically of Type Ic-BL, appearing at the location of the neutrino. The supernova would have an explosion time compatible with the neutrino detection time, and since SNe brighten over a period of days, this optical signature would be delayed relative to the neutrino itself.

(iii) **GRB afterglows.** Another signature of the supernova jet scenario would be the direct detection of a long-GRB afterglow. Models have also predicted neutrino emission for short GRBs, so a short-GRB afterglow could also be a potential counterpart (Waxman & Bahcall 1997). These GRB afterglows would not be detected before the neutrino detection, and would fade rapidly over the next few hours before falling below the ZTF detection threshold.

(iv) **AGN Flares**. AGN flares, and especially blazar flares, have been suggested as neutrino sources (Bednarek & Protheroe 1999), though the neutrino emission itself would not necessarily be directly correlated to the optical emission. For example, for the standard two-hump Spectral Energy Distribution (SED) model, the optical emission could serve primarily as a tracer for photon target density but not necessarily PeV proton luminosity. We restrict ourselves to searches for AGN undergoing significant optical flaring coincident with a neutrino. Neutrinos could also be produced in AGN without coincident optical flares, but such neutrino emission scenarios are not best probed with an optical follow-up programme such as ours.

(v) **Tidal disruption events**. TDEs have been suggested as neutrino sources, through multiple emission channels such as jets, outflows or in coronae (see Hayasaki 2021 for a recent review). The time-scale for neutrino production remains unclear, but would not be expected prior to the TDE itself. Non-thermal emission from TDEs can last several hundred days, so the signature in this case would be any 'ongoing' TDE coincident with a neutrino.

We do not enforce any additional cut on candidate distance, because IceCube detects neutrinos emitted throughout the universe rather than being restricted only to the local universe (see Strotjohann, Kowalski & Franckowiak 2019 for a more detailed explanation of this effect). However, given the limiting magnitude of ZTF, the candidates we find will nonetheless be biased towards lower redshifts.

We do not explicitly reject objects with a history of variability, because variable objects have been proposed as possible neutrino sources. However, our programme is intended to identify increased optical flux that is contemporaneous with a neutrino's detection, so only variable objects with significantly enhanced flux relative to reference images are selected by our pipeline. The blazar flare of TXS 0506+056 fell into this category (IceCube Collaboration et al. 2018), and we would be capable of identifying similar examples.

To date, the *NuZTF* pipeline has identified 172 candidates for visual inspection out of an observed area of 154.33 sq. deg across 24 neutrinos, using a search window of 14 d after each neutrino detection. This corresponds to an initial density of 1.05 candidates per sq. deg. of sky. The full list of candidates for each neutrino is given in the Appendix.

Visual inspection then enables us to further classify objects and reject background detections. Viewing difference images directly enables us to identify additional image artefacts. We select likely stars through cross-matches to *Gaia* (*Gaia* Collaboration et al. 2018), where we reject sources with significant (3σ) evidence for parallax, and to SDSS star/galaxy morphology classifications (Stoughton et al. 2002).

We then flag AGN through matches to catalogued sources in the Milliquas catalogue (Flesch 2021), or via WISE colour cuts (Wright et al. 2010; Stern et al. 2012). We further cross-match to NASA's NED data base, to flag any missing catalogued sources (Helou et al. 1991). We seek to distinguish between 'routine' AGN variability and extreme AGN flares. We search for evidence of flaring activity at the time of neutrino detection using the data provided in the ZTF alert packets (Patterson et al. 2019), which are based on difference images. For cases where a source appears to be significantly variable, or may have been flaring at the time of neutrino detection, we run dedicated forced photometry on the science images to produce a source light curve (Masci et al. 2019). We reject AGN with no evidence for contemporaneous flaring as 'AGN variability'. After removing those sources flagged as stars (17), image artefacts (17), or AGN variability (84), we are left with 54 'interesting candidates' (5 AGN flares, 12 confirmed transients, and 37 unclassified sources). The full breakdown in classification is shown in Fig. 2.

These interesting candidates include potential transients, which we seek to classify spectroscopically. Some objects will have already been classified serendipitously, in particular those brighter than 19.0 mag selected by the ZTF Bright Transient Survey (Fremling et al. 2020; Perley et al. 2020). The efficiency with which candidates were classified can be seen in Fig. 3. Above a peak apparent

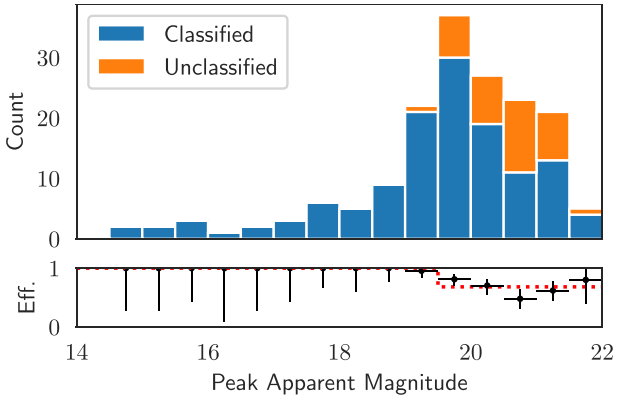

Figure 3. Top: apparent magnitude distribution of candidates selected for visual inspection. Bottom: classification efficiency as a function of peak apparent magnitude. The red-dashed line indicates our step-function approximation of classification efficiency.

Table 2. Summary of dedicated spectroscopic programmes for our neutrino follow-up programme.

Instrument	Programmes
SEDm	2018, 2019, 2020, 2021
NOT	2021B (OPT21B_50, PI: Franckowiak)
	2021B (P64-112)
	2021B (P61-501)
	2022A (22A013, PI: Franckowiak)
TNG	2021B (OPT21B_50, PI: Franckowiak)
	2022A (22A01, PI: Franckowiak)
GEMINI	2021A (GN-2021A-Q-116, PI: Kasliwal)
	2021B (GN-2021B-Q-117, PI: Kasliwal)
GTC	2020B (GTC73-20B, PI: Amaro Seoane)

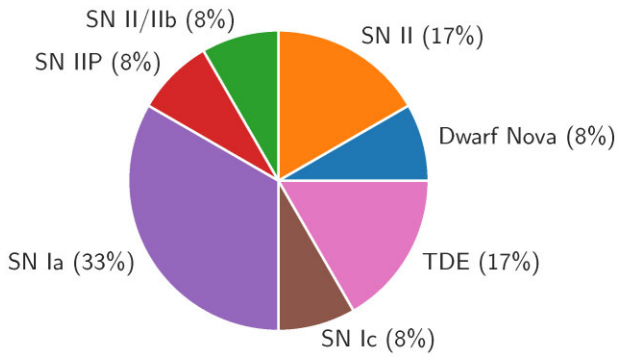

Figure 4. Breakdown of the 12 identified transients by subclass.

magnitude of 19.5, almost all candidates are classified. There were 106 fainter candidates in total, of which 68 per cent were classified. The spectroscopic programmes which supported our programme are listed in Table 2.

The transients are further broken down by subclass in Fig. 4. Four could be immediately excluded as candidates based on their classification as SNe Ia, a population not predicted to emit high-energy neutrinos. Of the remainder, beyond the two TDEs, no further sources exhibited electromagnetic signatures from the theoretically-predicted neutrino emission scenarios listed above. However, we cannot exclude the possibility that future theoretical work proposes

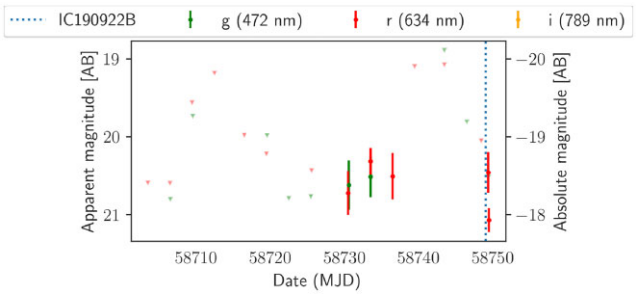

Figure 5. ZTF light curve of SN 2019pqh. The arrival time of neutrino IC190922B is marked by the dashed blue line.

additional neutrino emission scenarios not considered here, and therefore we cannot definitively rule out these transients as neutrino sources. We can state that none of them are consistent with existing models.

A selection of highlighted results is given in the following sections. We specifically list transients which were unclassified at the time of our ToO observations, and the additional follow-up that we took to confirm their nature. ZTF data for two other candidate neutrino sources from the literature, PKS 1502+106 and BZB J0955+3551, are also outlined in Section 5. We omit ZTF data for the probable neutrino-TDEs AT 2019dsg and AT 2019fdr, as these have already been released in dedicated publications (Stein et al. 2021b; Reusch et al. 2022). All other classified sources are listed in Appendix tables B1-B20.

For four neutrino campaigns (IC200107A, IC201007A, IC201222A, and IC210922A), no candidates were identified, and there are no corresponding lists in the appendix.

3 CANDIDATE TRANSIENT COUNTERPARTS

3.1 SN 2019pqh and IC190922B

Follow-up of IC190922B by ZTF identified the candidate supernova SN 2019pqh/ZTF19abxtupj (Stein et al. 2019d). The light curve is shown in Fig. 5, where upper limits are illustrated with triangles. The arrival time of the neutrino on 2019 September 22 is marked with a dotted line, and the supernova is detected in the subsequent ToO observations. The neutrino arrival time was close to optical peak, consistent with a CSM-interaction scenario.

However, a spectrum was taken by the *NUTS2 collaboration* (Holmbo et al. 2019), and the supernova was classified as a Type II supernova without spectroscopic signatures of CSM interaction (Reguitti et al. 2019). A higher-resolution spectrum of the object was also obtained on 2019 September 28, shown in Fig. 6, using the *Low Resolution Imaging Spectrometer* (LRIS) spectrograph at the Keck observatory (PI: Yan) (Oke et al. 1995). A historical spectrum of the host galaxy, taken by the *Sloan Digital Sky Survey* (SDSS; Abolfathi et al. (2018)), is also shown in Fig. 6. Both the transient and host galaxy exhibit prominent Balmer lines, highlighted in orange in Fig. 6, from which a redshift of 0.134 is derived. A template-matching classification using SNID (Blondin & Tonry 2007) confirms a Type II supernova classification, with the best match being a Type IIb supernova (SN 1993J, Barbon et al. 1995) 2 d before peak, also shown in Fig. 6.

With this redshift, a peak absolute magnitude of −18.6 was derived, atypically bright for such a Type II supernova (see e.g. Lyman et al. 2016). One explanation for this enhanced luminosity could be CSM interaction, through which additional ki-

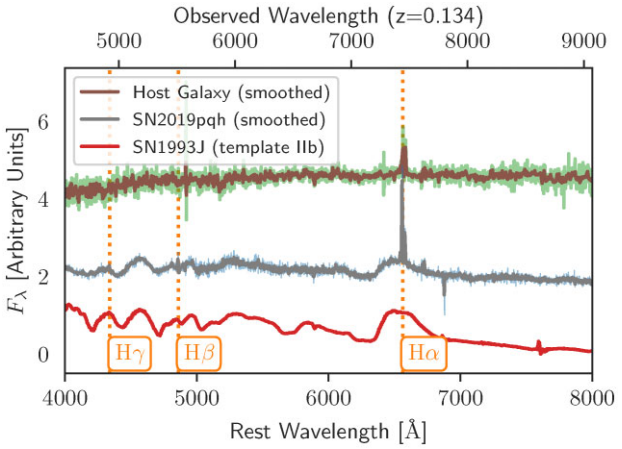

Figure 6. Spectrum of SN 2019pqh, taken on 2019 September 28. A historical spectrum of the host galaxy taken by SDSS, and a similar spectrum of a Type IIb supernova, are provided for comparison.

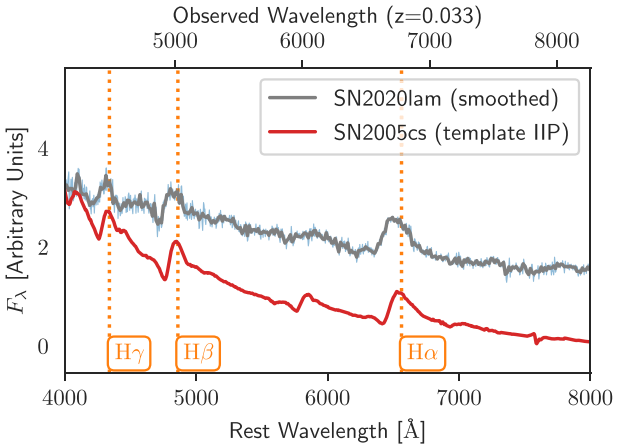

Figure 7. Spectrum of SN 2020lam, taken on 2020 June 06. A similar spectrum, from Type IIP supernova SN 2005cs, is shown for comparison.

netic energy is converted to electromagnetic emission. However, the lack of corresponding narrow line spectroscopic signatures generally disfavours the existence of CSM-interaction, and thus any associated neutrino emission from this object. It is therefore likely that SN 2019pqh is instead unrelated to the neutrino IC190922B.

3.2 SN 2020lam and IC200530A

ZTF serendipitously observed the localization of neutrino alert IC200530A on 2020 May 30, just 10 min after detection (Stein 2020e), as part of routine survey operations (Reusch et al. 2020b). Additional ToO observations were then conducted on 2020 May 31 in *g* and *r* band, and again on 2020 June 01. During ZTF follow-up of IC200530A, SN 2020lam/ZTF20abbpkpa was identified as a candidate supernova and potential optical counterpart (Reusch et al. 2020b). Spectroscopic observations were triggered using the NOT/ALFOSC spectrograph on 2020 June 06 (PI: Sollerman), which confirmed SN 2020lam as a Type II supernova (Reusch et al. 2020c) using SNID. This spectrum is shown in Fig. 7, alongside the matching Type IIP supernova (SN 2005cs, Pastorello et al. 2006) mapped to the same redshift.

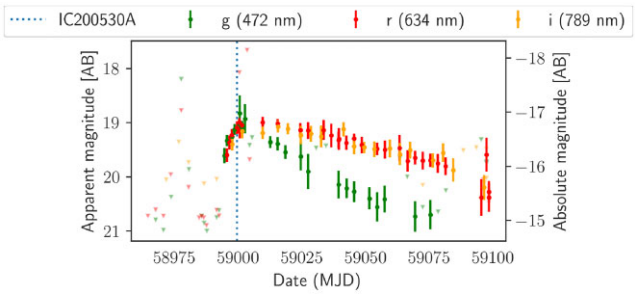

Figure 8. ZTF light curve of SN 2020lam. The arrival time of neutrino IC200530A is marked by the dashed blue line.

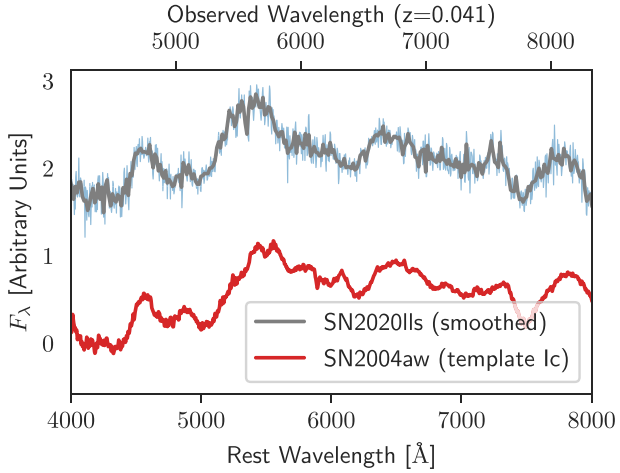

Figure 9. Spectrum of SN 2019lls, taken on 2020 June 13. A similar spectrum, of Type Ic supernova SN 2004aw, is shown for comparison.

As seen in the light curve in Fig. 8, the supernova was close to peak at neutrino detection time. The object then rapidly cooled, and thus reddened, as is typical for supernovae. Given the neutrino arrival time, CSM-interaction would be the only viable neutrino production mechanism. However, the spectrum shown in Fig. 7 had no narrow lines, and therefore did not provide any evidence supporting such CSM interaction. SN 2020lam was therefore likely unrelated to IC200530A.

3.3 SN 2020lls and IC200530A

SN 2020lls/ZTF20abdnpdo was also identified as a candidate supernova on 2020 May 30, during ZTF follow-up of IC200530A (Reusch et al. 2020b). Spectroscopic observations were again triggered using the NOT/ALFOSC spectrograph on 2020 June 12 (PI: Sollerman), which confirmed that SN 2020lls was a Type Ic supernova without broad-line features (Reusch et al. 2020d). This spectrum is illustrated in Fig. 9, alongside a matching Type Ic supernova spectrum from SNID mapped to the same redshift (Taubenberger et al. 2006). Given that the supernova had not been detected in alert data prior to the neutrino arrival time, and that it belonged to the subpopulation associated with relativistic jets, SN 2020lls was a candidate for the choked-jet neutrino production model.

However, as can be seen in Fig. 10, forced photometry analysis (Reusch 2020) revealed a lower-threshold *i*-band ZTF detection preceding the neutrino arrival. Additionally, modelling of the light curve using the *MOSFIT* software (Guillochon et al. 2018) revealed an estimated explosion date predating the neutrino by a week. In

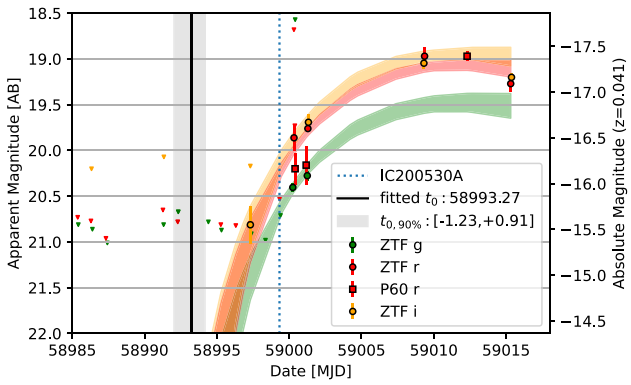

Figure 10. ZTF light curve of SN 2020lls. The arrival time of neutrino IC200530A is marked with the blue-dotted line. The supernova model fit from *MOSFIT* is indicated by the shaded orange/red/green bands, and the the best-fit explosion time is given by the vertical black line.

combination, these results disfavoured any supernova explosion origin for the neutrino, suggesting that SN 2020lls was instead unrelated to IC200530A (Reusch et al. 2020d).

4 AGN FLARE CANDIDATES

While the vast majority of AGN detections from our pipeline were categorized as 'AGN variability', visual inspection revealed five AGN which appeared to possibly undergo optical flaring at the time of neutrino detection. The forced photometry light curves of these five flares are shown in Fig. 11. We attempt to quantify whether the optical light curves of these AGN identify them as candidate neutrino sources.

We can consider possible optical signatures associated with neutrino emission. One scenario is the optical flaring observed for TXS 0506+056 during the detection of neutrino IC170922A (IceCube Collaboration et al. 2018). In particular, the optical apparent V-band magnitude of TXS 0506+056 was observed to increase from 15.0 to 14.5 during the time of neutrino detection, corresponding to a flux increase of >50 per cent, over a period of 50 d, relative to the pre-neutrino baseline.

AGN can also exhibit short-term variability for periods of hours or days, but we caution that the detection of a high-energy neutrino alert is a process that requires a substantial fluence at the IceCube detector, even after accounting for the significant Eddington bias associated with cosmic neutrino detection (Strotjohann et al. 2019). The corresponding neutrino flux that is required is inversely proportional to the duration of neutrino emission, and therefore associating a neutrino detection with a temporary electromagnetic signature lasting hours or days would imply an extremely high average neutrino flux for the duration of that signature. Such highly luminous rapid neutrino flares are not well motivated theoretically, it is therefore unlikely that short AGN flares are indicators of neutrino production.

In contrast, longer-term electromagnetic signatures can serve as tracers for neutrino emission. For example, month-long flaring periods of substantially elevated flux can dominate the neutrino emission of blazars (see e.g. Rodrigues et al. 2021). Very long flares, with durations of years, could also be relevant for neutrino production. However, given the relatively short baseline of ZTF observations, our neutrino follow-up programme is not well-suited to identify them. We therefore restrict ourselves to searching for such month-long optical flares, as was observed for TXS 0506+056.

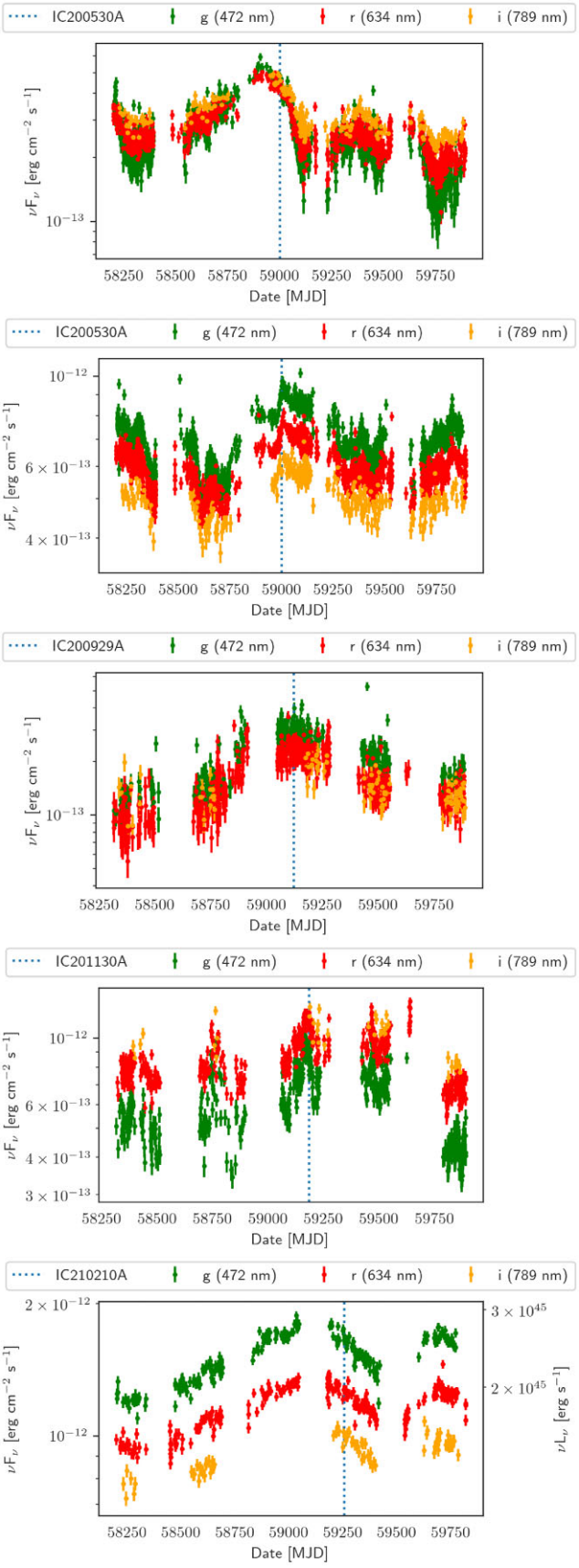

Figure 11. ZTF light curve of five AGN flares coincident with high-energy neutrinos. From top to bottom, the sources are: ZTF18aavecmo, ZTF18abrwqpr, ZTF20aamoxyt, ZTF18abxrpgu, and ZTF19aasfvqm.

Table 3. Summary of the 5 AGN flares coincident with neutrinos, including the instantaneous flux during neutrino detection, median flux over the entire ZTF baseline, and the ratio of these values.

Object	Filter	Inst. flux [10^{-13} erg cm^{-2} s^{-1}]	Med. flux [10^{-13} erg cm^{-2} s^{-1}]	Inst. flux/med. flux
ZTF18aavecmo	g	4.5	2.5	1.82
ZTF18aavecmo	r	4.3	2.6	1.67
ZTF18aavecmo	i	4.5	3.2	1.40
ZTF18abrwqpr	g	9.0	6.9	1.31
ZTF18abrwqpr	r	7.2	5.8	1.24
ZTF18abrwqpr	i	6.0	5.0	1.21
ZTF20aamoxyt	g	3.2	2.3	1.38
ZTF20aamoxyt	r	2.4	1.6	1.51
ZTF18abxrpgu	g	8.9	6.7	1.33
ZTF18abxrpgu	r	11.2	8.9	1.27
ZTF19aasfvqm	g	16.5	14.7	1.12
ZTF19aasfvqm	r	12.6	11.6	1.08
ZTF19aasfvqm	i	10.0	8.8	1.14

We calculate the median flux for each of the five AGN, and each ZTF filter, in a ± 25 d window centred on the neutrino detection. We divide this instantaneous flux by the median flux of the source in that filter over the entire $\sim$4 yr ZTF baseline, giving a proxy for relative optical flare strength. These values are given in Table 3. Of the five AGN, only two (ZTF18aavecmo and ZTF20aamoxyt) had a median instantaneous flux >50 per cent above the baseline median flux. ZTF18aavecmo reached this threshold in both g and r band, while ZTF20aamoxyt reached this threshold only in r. We conclude that the remaining three AGN (ZTF18abrwqpr, ZTF18abxrpgu, ZTF19aasfvqm) do not exhibit substantial neutrino-coincident optical flares, and we therefore find no evidence to suggest they are counterparts to high-energy neutrinos.

ZTF18aavecmo (top panel of Fig. 11), cross-matched to source WISEA J170539.32+273641.2, is classified as a likely QSO in the Milliquas catalogue. It underwent a single coherent flare lasting approximately one year, with a peak flux roughly triple the quiescent flux measured by ZTF. It was coincident with neutrino IC200530A, detected during the decay of the optical flare. However, this flare was extremely faint, with a median flux at the time of neutrino detection was $\nu F_\nu \approx 5 \times 10^{-13}$ erg cm^{-2} s^{-1}. This is a factor of 20 lower than the flux observed for TXS 0506+056 during the detection of IC170922A (IceCube Collaboration et al. 2018).

ZTF20aamoxyt (middle panel of Fig. 11) is a likely AGN flare, detected coincident with IC200929A. It appears to be spatially consistent with its host galaxy nucleus, and cross-matched to WISEA J015853.53+035126.6. Based on a WISE colour of W1−W2 = 0.7, it is a possible AGN. The neutrino IC200929A was detected during an extended year-long flare. Much like ZTF18aavecmo, ZTF20aamoxyt at the time of neutrino detection was substantially fainter than TXS 0506+056, with a median flux of $\nu F_\nu \approx 3 \times 10^{-13}$ erg cm^{-2} s^{-1}.

We thus identify no optical AGN flares which resemble the multiwavelength flare of TXS 0506+056 in 2017, from any of our 24 neutrino follow-up campaigns. We emphasize that our results do not preclude a significant degree of neutrino emission from AGN more broadly, but they do disfavour scenarios where the vast majority of astrophysical neutrinos are produced by bright AGN optical flares. There is no tension with scenarios where AGN neutrino emission is not dominated by bright optical flares, for example the 'steady state' AGN neutrino models tested in Abbasi et al. (2022) or scenarios where AGN neutrino emission is correlated only to gamma-ray flares. Constraining such scenarios would require more comprehensive multiwavelength analysis of AGN light curves, incorporating other wavelengths in addition to the optical data presented here. A more systematic study of correlations between ZTF-detected AGN flares and neutrinos, including corresponding chance coincidence probabilities, will be the subject of a future analysis.

5 CANDIDATE NEUTRINO SOURCES FROM THE LITERATURE

We here provide data on two candidate neutrino sources reported in the literature. However, we caution that none of the objects presented here were selected by our pipeline as ZTF candidates, and therefore are not considered part of our systematic search for neutrino counterparts. We would not claim any such object as a candidate neutrino sources in our neutrino follow-up programme, because the chance coincidence probability would be unquantifiable. Any search for additional candidate neutrino sources, beyond those candidates found by our pipeline following ToO observations, would require an independent and unbiased systematic analysis procedure.

5.1 PKS 1502+106

The neutrino IC190730A was reported by IceCube in spatial coincidence with PKS 1502+106 (Stein 2019a), a particularly gamma-bright Flat Spectrum Radio Quasar (FSRQ) with a catalogued redshift of $z = 1.84$ (Albareti et al. 2017). The object was observed by ZTF as part of ToO observations, and was detected under the ZTF candidate name ZTF18aaqnqzx (Stein et al. 2019c). The blazar had already been repeatedly detected as part of the routine survey operations, with both positive and negative flux changes relative to survey reference images.

The blazar light curve is shown in Fig. 12, using data from science images with the ZTF forced photometry service (Masci et al. 2019). The neutrino arrival time is marked in blue. There was no significant flaring observed for this source coincident with the neutrino. The blazar at this point was dimmer than survey reference images, with the neutrino arriving during a year-long fading, and consequently was not selected by our follow-up pipeline as a possible counterpart. There is thus no evidence from the contemporaneous

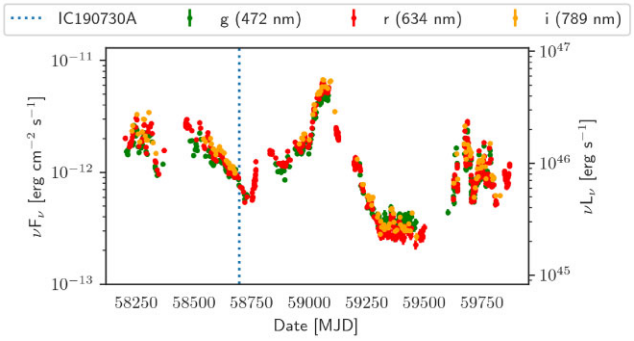

Figure 12. ZTF light curve of blazar PKS 1502+106. The arrival time of neutrino IC190730A is marked with the vertical-dashed line.

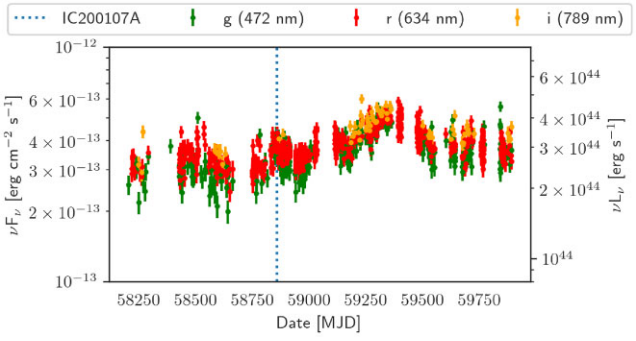

Figure 13. ZTF light curve of blazar BZB J0955+3551. The arrival time of neutrino IC200107A is marked with the vertical dashed line.

ZTF data to suggest a causal connection between IC190730A and PKS 1502+106, consistent with data from other observatories which did not see any evidence of short-term flaring (Franckowiak et al. 2020).

Data from the Owens Valley Radio Observatory (OVRO) did reveal that the radio flux was elevated in the months preceding the neutrino detection relative to the decade-long observation baseline, behaviour which has also been claimed for TXS 0506+056 and other neutrino-coincident blazars (Kiehlmann et al. 2019). Comprehensive time-dependent modelling has found that the detection of a neutrino alert from PKS 1502+106 is consistent with the multiwavelength observations of this object, so a neutrino-blazar association is plausible but likely unrelated to the flaring activity (Oikonomou et al. 2021; Rodrigues et al. 2021). In any case, the new optical data presented here can be used to further constrain such neutrino emission scenarios.

5.2 BZB J0955+3551

IC200107A was a high-energy neutrino reported by IceCube (Stein 2020a) which was later identified to be in spatial and temporal coincidence with a blazar undergoing a dramatic simultaneous X-ray flare (Krauss et al. 2020; Giommi, Glauch & Resconi 2020c). The source BZB J0955+3551 (also known as 4FGL J0955.1+3551 and 3HSP J095507.9+355101), located at a redshift of 0.55703 (Paliya et al. 2020), belongs to the specific subclass of extreme blazars, which are characterized by synchrotron peaks at very high frequencies, which had been proposed as especially promising candidates of high-energy neutrinos (Padovani et al. 2016).

More comprehensive multifrequency modelling has confirmed that the detection of a neutrino alert from an extreme blazar is plausible, though the simultaneous X-ray flare may not be directly related to the neutrino production (Paliya et al. 2020; Petropoulou et al. 2020; Giommi et al. 2020b). The ZTF light curve for BZB J0955+3551 is shown in Fig. 13. There is no evidence of any optical flaring on short or long time-scales coincident with the detection of IC200107A.

6 LIMITS ON NEUTRINO SOURCE POPULATIONS

With our programme, we did not find any likely candidate counterparts from any population except TDEs. We can consider limits that can be placed on other potential sources of astrophysical neutrinos given the non-detections. These limits will clearly not apply for TDEs, because for this population probable counterparts were detected. If AT 2019fdr is ultimately found not to be a TDE, for example if it instead an SLSN (Pitik et al. 2022), the limits would not apply to that population either. It will however apply to all other populations which would be detected by ZTF, provided at least one detection occurred within the 14 d window after neutrino arrival time. Our search has no requirement that an optical light-curve peaks after the neutrino detection, so these limits also apply to older/fading transients.

For each neutrino, we can consider the probability that an astrophysical counterpart would be detected. A counterpart could only be detected if a given IceCube neutrino was astrophysical, with this as P_{astro} probability being reported by IceCube in GCN notices as the '*signalness*' parameter. For each neutrino that was indeed astrophysical, the source could only then be detected if it lay within the area observed by ZTF. We can estimate this probability, P_{obs}, by assuming that the 90 per cent probability is uniformly distributed across the rectangle reported by IceCube, A_{IC}, such that:

$$P_{\rm obs} = 0.9 \times \frac{A_{\rm ZTF}}{A_{\rm IC}}, \tag{1}$$

where A_{ZTF} is the area observed by ZTF after accounting for detector chip gaps.

The probability to find an optical counterpart is then given by the joint probability that the neutrino is astrophysical, P_{astro}, that the astrophysical source lay in the observed ZTF area, P_{obs}, and the probability that a given counterpart would be detectable with our programme $P_{detectable}$. The values of P_{astro} and P_{obs} for each alert are given in Table 4.

The detectable probability will depend on the selection efficiency, ϵ_{det}, of our programme. This selection efficiency in turn depends on the apparent magnitude of the electromagnetic counterpart. Motivated by our classification efficiency in Fig. 3, we assume completeness for objects brighter than 19.5 mag, and a classification efficiency of 68 per cent for objects fainter than this (this assumption is illustrated with the red-dashed line in Fig. 3). We additionally assume a conservative 95 per cent detection efficiency for sources to be found by our pipeline, if said source was imaged by the camera. Chip gaps in the detector are already accounted for in equation (1). Because the detection efficiency will decrease as the objects approach the ZTF limiting magnitude of 21.5 for 300 s exposures, we neglect objects fainter than 21 mag in our calculation:

$$\epsilon_{\rm selection}(m) = 0.95 \times \begin{cases} 1.00 & m \leq 19.5 \\ 0.68 & 19.5 \leq m \leq 21.0 \\ 0.00 & 21.0 \leq m \end{cases} \tag{2}$$

The fraction of astrophysical neutrino sources that are detected by our programme will depend on the properties of a given population.

Table 4. Probability of finding a counterpart for each neutrino, assuming counterparts are sufficiently bright to be detected by our ZTF neutrino follow-up programme.

Event	P_{astro}	P_{obs}	$P_{astro} \times P_{obs}$
IC190503A	0.36	0.64	0.23
IC190619A	0.55	0.71	0.39
IC190730A	0.67	0.75	0.50
IC190922B	0.51	0.82	0.42
IC191001A	0.59	0.81	0.48
IC200107A	0.50	0.74	0.37
IC200109A	0.77	0.89	0.69
IC200117A	0.38	0.84	0.32
IC200512A	0.32	0.85	0.27
IC200530A	0.59	0.78	0.46
IC200620A	0.32	0.65	0.21
IC200916A	0.32	0.77	0.25
IC200926A	0.44	0.66	0.29
IC200929A	0.47	0.70	0.33
IC201007A	0.88	0.87	0.77
IC201021A	0.30	0.82	0.25
IC201130A	0.15	0.75	0.11
IC201209A	0.19	0.61	0.12
IC201222A	0.53	0.82	0.43
IC210210A	0.65	0.67	0.43
IC210510A	0.28	0.82	0.23
IC210629A	0.35	0.69	0.24
IC210811A	0.66	0.76	0.50
IC210922A	0.93	0.67	0.62

For a power-law neutrino spectrum, the differential neutrino particle flux at Earth for a transient population with a redshift-independent luminosity distribution is proportional to

$$\frac{dF(z)}{dz} = \frac{dN(z)}{dEdAdtdz} \propto \left[(1+z)^{2-\gamma} \times \frac{R(z)}{4\pi D_L^2} \right] \frac{dV_C}{dz}, \quad (3)$$

where γ is the intrinsic neutrino spectral index such that $\frac{dN_\nu}{dE} \propto E^{-\gamma}$, $R(z) = \rho(z)/\rho(0)$ is the normalized source redshift evolution for a population with rate $\rho(z)$, D_L is the luminosity distance, and V_C is the comoving volume (see e.g Murase (2007)). By normalizing equation (3), we can derive a probability density function (PDF) for the redshift of detected neutrinos:

$$P_{\rm dist}(z) = \frac{dF(z)}{dz} \Big/ \left(\int_0^\infty \frac{dF(z)}{dz} dz \right) \quad (4)$$

PDFs for $P_{\rm dist}(z)$, calculated using the *flarestack* code (Stein et al. 2020a) for an E^{-2} spectrum, are shown in Fig. 14 for redshift evolutions from a 'GRB-like' population (Lien et al. 2014) and from a Star-Formation-Rate population ('SFR-like') (Strolger et al. 2015). We also show a blazar-like redshift evolution assuming a 'primarily-density evolution' (PDE) following the formulation of Ajello et al. (2015), motivated by recent observations favouring such a distribution (Marcotulli, Di Mauro & Ajello 2020). The blazar redshift distribution is expected to vary with underlying source luminosity, so we assume a blazar gamma-ray luminosity of $L_\gamma \approx 10^{46}$ erg s^{-1}, motivated by observations of TXS 0506+056 (Padovani et al. 2018), and the best-fit parameters for a PDE blazar evolution from Ajello et al. (2015).

It can be seen in Fig. 14 that GRB-like populations tend to be at greater distances than SFR-like ones, with GRB-like neutrinos being emitted from a median redshift of $z = 1.34$, whereas SFR-like neutrinos would have a median distance of $z = 0.64$ and blazar-like neutrinos would have a similar median of $z = 0.57$. This has a direct impact on the population properties compatible with our limits, because a neutrino population dominated by nearby sources will generally produce counterparts with brighter apparent magnitudes.

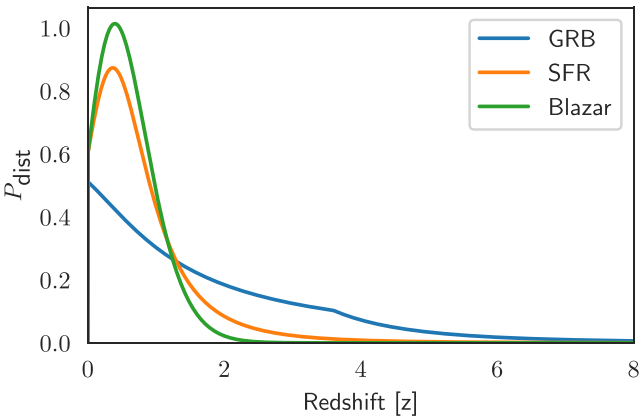

Figure 14. PDF for neutrino sources as a function of redshift, for both GRB-like and SFR-like source evolutions.

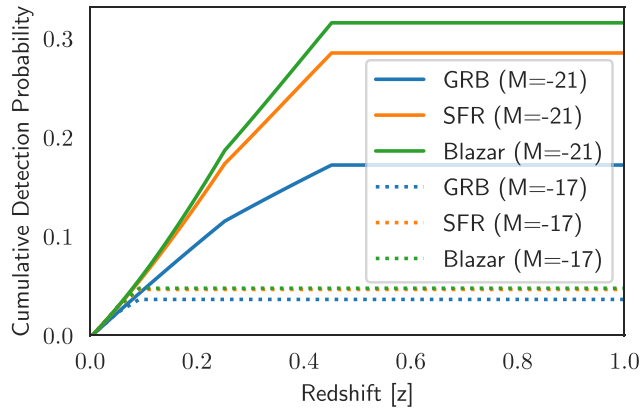

Figure 15. Cumulative counterpart detection probability as a function of redshift.

For a given source evolution, the probability of detecting a counterpart will then ultimately depend on the underlying luminosity function of the population. For an absolute magnitude, M, the counterpart detection probability is equal to the integrated product of the probability that a counterpart has a given redshift, $P_{\rm dist}(z)$, and the detection efficiency of our programme for the apparent magnitude, $m(M, z)$, corresponding to that redshift:

$$P_{\rm detectable}(M) = \int_0^\infty \left[\epsilon_{\rm det}(m(M,z)) \times P_{\rm dist}(z) \right] dz \quad (5)$$

The impact of different evolutions and absolute magnitudes can be seen in Fig. 15. For sources with an absolute magnitude of -21, our programme would be sensitive to counterparts up to a redshift of $z \approx 0.45$, beyond which $m > 21$ so $\epsilon_{\rm selection} = 0$. For an SFR-like evolution, this would correspond to $P_{\rm detectable}(-21) = 26$ per cent, but for the higher-z GRB-like neutrino distribution, we would instead find $P_{\rm detectable} = 16$ per cent. For a fainter absolute magnitude of -17, our programme would probe a much smaller volume up to redshift $z \approx 0.1$, so then $P_{\rm detectable}$ would be 5 and 4 per cent for SFR-like and GRB-like populations, respectively.

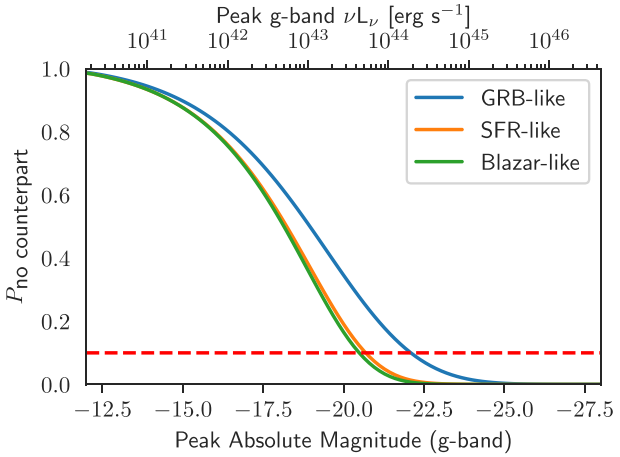

Figure 16. Probability of detecting no counterpart as a function of absolute magnitude for $f = 1$. The dotted line corresponds to 90 per cent confidence.

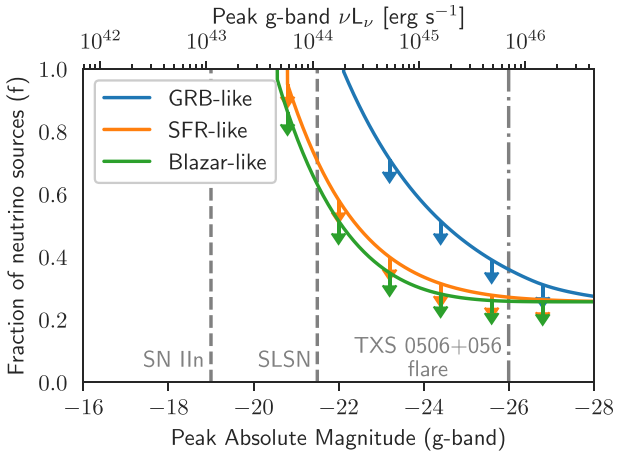

Figure 17. Upper limits (90 per cent CL) on the luminosity function of neutrino sources.

Combining these values, the joint probability for us to find a counterpart during a follow-up campaign is given by

$$P_{\rm find}(f, M) = P_{\rm astro} \times P_{\rm obs} \times P_{\rm detectable}(M) \times f(M), \quad (6)$$

where f is the fraction of astrophysical neutrino sources with an absolute magnitude equal to or brighter than M. The probability that no counterpart was detected in any of our 24 follow-up observations is then given by

$$P_{\rm no\_counterpart}(M, f) = \prod_{i=1}^{24} \left(1 - P_{\rm find,\,i}(M, f)\right) \quad (7)$$

The probability of no counterpart detection is given in Fig. 16 as a function of M. The results of our programme strongly disfavour scenarios where all neutrino sources have bright absolute magnitudes. The horizontal dashed line in Fig. 16 represents a 10 per cent chance of non-detection, and thus a 90 per cent confidence limit. We can use this threshold to set a limit on the luminosity function of neutrino sources, by choosing the appropriate fraction f such that $P_{\rm nocounterpart}(M, f) > 0.1$.

These constraints on $f(M)$ at 90 per cent CL are illustrated in Fig. 17, for the two source evolutions. These are generic constraints on the underlying luminosity function of neutrino sources, and are agnostic to the actual nature of the neutrino sources which follow the redshift evolutions. They constrain the aggregate neutrino flux emitted by, for example, a SFR-like population, and thus apply equally well to a composite neutrino flux with, for example, multiple SFR-like neutrino populations. To the best knowledge of the authors, this is the first time generic constraints on the optical luminosity function of neutrino sources have been derived, though a similar procedure has already been used to derive limits from optical searches for counterparts to gravitational waves (Kasliwal et al. 2020). One novel consequence of these general limits are the first observational constraints on the contribution of the brightest superluminous supernova to the diffuse neutrino flux, under the assumption these trace the star formation rate. Objects brighter than an absolute magnitude of −22 can contribute no more than 58 per cent of the total astrophysical neutrino alerts if SFR-like.

During the multiwavelength flare of TXS 0506+056 which coincided with the detection of neutrino IC170922A, the source exhibited a g-band optical flux of ∼6 mJy m^{-1} = 14.5 (IceCube Collaboration et al. 2018), more than double the mean archival g-band magnitude of 2.7 mJy m^{-1} = 15.3 in Pan-STARRS1 (Chambers et al. 2016). This would correspond to a transient flare of absolute magnitude M_g ≈-26 in difference imaging. Blazar flares such as this can contribute no more than 26 per cent of the total neutrino flux.

It should be noted that none of these values account for the impact of dust extinction, which would shift the curves in Fig. 17 rightwards to higher luminosities. However, we do not expect that this would significantly impact the results presented here. Our limits are only valid for a given source evolutions, and would need to be adjusted for alternative ones. For example, if the neutrino source evolution were strongly negative (lower number density at higher redshift), a larger fraction of the flux would arise from local sources. Therefore, our limits would instead be more constraining.

It should also be noted that these limits assume that a given transient could pass our selection criteria outlined in Section 2, and therefore do not apply to extremely rapid transients such as GRB afterglows, which peak and fade on time-scales ≲1 d. Such objects are not well captured by the ZTF public survey cadence or our typical neutrino follow-up observation cadence, and are unlikely to be detected multiple times in order to pass our selection criteria, so our detection efficiency will be somewhat lower.

7 CONCLUSIONS

The ZTF neutrino follow-up programme coincided with the introduction of the upgraded IceCube alert selection, yielding one unretracted alert every 2 weeks and one ZTF follow-up campaign every 4 weeks on average. The programme resulted in the identification of two probable neutrino sources (Stein et al. 2021b; Reusch et al. 2022), and the first limits on the optical luminosity function of neutrino sources.

Though the limits presented here constrain only the very brightest transients such as superluminous supernovae (SLSNe), they will continue to become more stringent over time if no new counterparts are identified. As can be seen in Fig. 18, extrapolating our analysis to a neutrino sample that was twice or four times as large would lead to substantially more constraining limits, and will be achieved on the present trajectory with 2 or 6 additional years of observations.

Although the data analysis presented considered candidates detected up to 14 d after neutrino detection, our early real-time counterpart searches generally focused on counterparts detected in the ToO observations scheduled for the first two nights after neutrino detection. Motivated by the systematic analysis performed here, and to improve sensitivity to time-delayed optical signatures such as

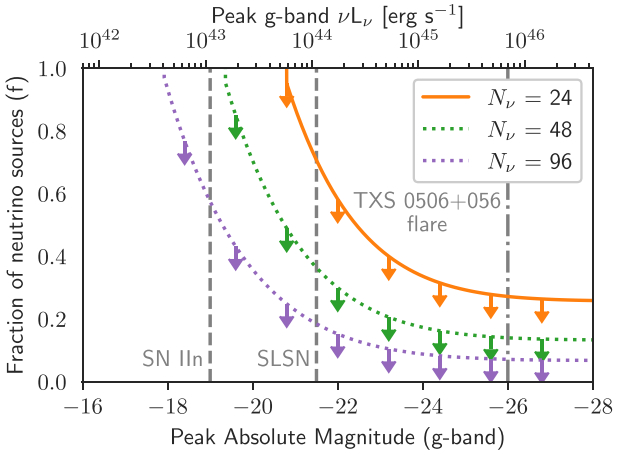

Figure 18. Upper limits (90 per cent CL) on the luminosity function of neutrino sources for an SFR-like evolution that would be derived for a ZTF neutrino sample that was twice ($N_\nu = 48$) or four times ($N_\nu = 96$) the size of the sample presented here.

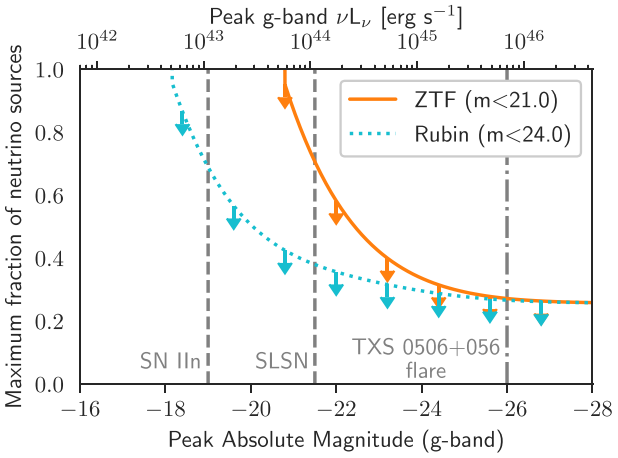

Figure 19. Upper limits (90 per cent CL) on the luminosity function for an SFR-like population with our sample of 24 observed neutrino alert and our classification efficiency (ZTF), and limits that would be obtained for a comparable neutrino follow-up programme with the upcoming Rubin Observatory.

neutrino emission from choked jets, we have modified our ToO observation strategy to better cover a range of transient time-scales. We now trigger deep 300 s in g and r band on the first night of observations to obtain deep upper limits or faint detections, and to additionally yield colour information for any active transient. However, we replaced our second pair of 300 s exposures with a series of 30 s exposures spread over subsequent nights, to complement the public survey and ensure good coverage of the photometric evolution of candidates. Forced photometry is only possible for images from the public survey after they have been published as part of the regular ZTF Data Releases, but with this ToO monitoring we can perform forced photometry analysis in real time (Reusch 2020). We can also better prioritize spectroscopic follow-up with photometric classification.

One shortcoming of the ZTF programme thus far has been the relatively poor sensitivity to very rapid transients such as GRB afterglows, owing to the median latency of 12.2 h to first coverage. We plan to implement automated triggering with ZTF, similar to that operated by other observatories such as ASAS-SN (Necker et al. 2022), enabling low-latency observations for at least some favourable neutrino alerts with appropriate accessibility. Dedicated analysis of low-latency follow-up campaigns would yield more stringent constraints on GRB afterglows as neutrino sources.

The results and analysis presented here can serve as a pathfinder for future triggered neutrino follow-up programmes with wide-field instruments. In particular, ToO observations with the upcoming Vera C. Rubin Observatory would offer an unprecedented opportunity to probe neutrino sources to much higher redshifts (Ivezić et al. 2019). Multiband observation coverage would enable photometric classification of many candidates, substantially extending the classification efficiency presented in Fig. 3 to much greater depths. An illustration of this is presented in Fig. 19, assuming that the same neutrino sample in Table 1 had instead been observed with the Rubin Observatory. For a comparable 60 per cent classification efficiency down to 24th mag, the corresponding limits on the neutrino luminosity function would be much more constraining for lower magnitudes. However, for very luminous optical sources such as blazar flares, the performance of both surveys for such a neutrino sample would be comparable. Given that there are only expected to be ∼12 astrophysical neutrinos in our sample, observations will never be able to overcome the 90 per cent limit from Poisson counting statistics even if they had a perfect 100 per cent efficiency. Instead, as seen in Fig. 18, only larger neutrino samples can enable stricter limits on bright sources.

Beyond optical observatories, similar electromagnetic neutrino follow-up programmes are planned for telescopes currently under construction. These include near-infrared (NIR) wavelengths with WINTER (Frostig et al. 2020; Lourie et al. 2020), at ultraviolet (UV) wavelengths with ULTRASAT (Sagiv et al. 2014), and in gamma-rays with CTA (Cherenkov Telescope Array Consortium et al. 2019; Carosi et al. 2021). These new instruments, in concert with the continuation of existing follow-up programmes, will enable us to study the dynamic neutrino sky across the entire electromagnetic spectrum.

ACKNOWLEDGEMENTS

RS and AF acknowledges support by the Initiative and Networking Fund of the Helmholtz Association through the Young Investigator Group programme (AF). AF acknowledges funding from the German Science Foundation DFG, via the Collaborative Reasearch Centre SFB1491 "Cosmic Interacting Matters – From Source to Signal. JN and SR acknowledges support by the Helmholtz Weizmann Research School on Multimessenger Astronomy, funded through the Initiative and Networking Fund of the Helmholtz Association, DESY, the Weizmann Institute, the Humboldt University of Berlin, and the University of Potsdam. ECK acknowledges support from the G.R.E.A.T research environment funded by *Vetenskapsrådet*, the Swedish Research Council, under project number 2016–06012, and support from The Wenner-Gren Foundations.

Based on observations obtained with the Samuel Oschin Telescope 48-inch and the 60-inch Telescope at the Palomar Observatory as part of the ZTF project. ZTF is supported by the National Science Foundation under Grant Number AST-1440341 and AST-2034437, and a collaboration including Caltech, IPAC, the Weizmann Institute of Science, the Oskar Klein Centre at Stockholm University, the University of Maryland, the University of Washington, Deutsches Elektronen-Synchrotron and Humboldt University, Los Alamos National Laboratories, the TANGO Consortium of Taiwan, the University of Wisconsin at Milwaukee, Lawrence Berkeley

National Laboratories, Trinity College Dublin, Lawrence Livermore National Laboratories, IN2P3, France, the University of Warwick, the University of Bochum, and Northwestern University. Operations are conducted by COO, IPAC, and UW. SED Machine is based upon work supported by the National Science Foundation under Grant Number 1106171. The ZTF forced-photometry service was funded under the Heising-Simons Foundation grant number 12540303 (PI: Graham).

The data presented herein were obtained in part at the W. M. Keck Observatory, which is operated as a scientific partnership among the California Institute of Technology, the University of California, and the National Aeronautics and Space Administration (NASA). The Observatory was made possible by the generous financial support of the W. M. Keck Foundation.

The authors wish to recognize and acknowledge the very significant cultural role and reverence that the summit of Mauna Kea has always had within the indigenous Hawaiian community. We are most fortunate to have the opportunity to conduct observations from this mountain.

Based on observations made with the Nordic Optical Telescope, owned in collaboration by the University of Turku and Aarhus University, and operated jointly by Aarhus University, the University of Turku and the University of Oslo, representing Denmark, Finland and Norway, the University of Iceland and Stockholm University at the Observatorio del Roque de los Muchachos, La Palma, Spain, of the Instituto de Astrofisica de Canarias. The data presented here were obtained in part with ALFOSC, which is provided by the Instituto de Astrofisica de Andalucia (IAA) under a joint agreement with the University of Copenhagen and NOT.

This research made use of Astropy, a community-developed core PYTHON package for Astronomy (Astropy Collaboration et al. 2013, 2018). This research made use of Astroquery (Ginsburg et al. 2019), of the NASA/IPAC Extragalactic Data base (NED) which is operated by the Jet Propulsion Laboratory, California Institute of Technology, under contract with the NASA.

8 DATA AVAILABILITY

The data presented here, and the Python analysis code used to generate the figures and key results, are available on Github:

https://github.com/robertdstein/nuztfpaper

They are also available directly from the author upon reasonable request.

REFERENCES

Aartsen M. G., et al., 2015, ApJ, 811, L52
Aartsen M. G., et al., 2017, Astropart. Phys., 92, 30
Aartsen M. G., et al., 2020, Phys. Rev. Lett., 124, 051103
Abbasi R., et al., 2022, Phys. Rev. D, 106, 022005
Abolfathi B., et al., 2018, ApJS, 235, 42
Ajello M., et al., 2015, ApJ, 800, L27
Albareti F. D., et al., 2017, ApJS, 233, 25
Astropy Collaboration, et al., 2013, A&A, 558, 33
Astropy Collaboration, et al., 2018, AJ, 156, 123
Barbon R., Benetti S., Cappellaro E., Patat F., Turatto M., Iijima T., 1995, A&AS, 110, 513
Bednarek W., Protheroe R. J., 1999, MNRAS, 302, 373
Bellm E. C., et al., 2019a, PASP, 131, 018002
Bellm E. C., et al., 2019b, PASP, 131, 068003
Blaufuss E., 2018a, GCN Circular, 23214
Blaufuss E., 2018b, GCN Circular, 23375
Blaufuss E., 2018c, GCN Circular, 23398
Blaufuss E., 2019a, GCN Circular, 23785
Blaufuss E., 2019b, GCN Circular, 23876
Blaufuss E., 2019c, GCN Circular, 24378
Blaufuss E., 2019d, GCN Circular, 24674
Blaufuss E., 2019e, GCN Circular, 24854
Blaufuss E., 2019f, GCN Circular, 24910
Blaufuss E., 2019g, GCN Circular, 25057
Blaufuss E., 2019h, GCN Circular, 25806
Blaufuss E., 2019i, GCN Circular, 26258
Blaufuss E., 2019j, GCN Circular, 26276
Blaufuss E., 2020a, GCN Circular, 27612
Blaufuss E., 2020b, GCN Circular, 27787
Blaufuss E., 2020c, GCN Circular, 27941
Blaufuss E., 2020d, GCN Circular, 28163
Blaufuss E., 2020e, GCN Circular, 28433
Blaufuss E., 2020f, GCN Circular, 28509
Blaufuss E., 2020g, GCN Circular, 28616
Blaufuss E., 2020h, GCN Circular, 28887
Blaufuss E., 2020i, GCN Circular, 28892
Blaufuss E., 2020j, GCN Circular, 29102
Blaufuss E., 2020k, GCN Circular, 29120
Blaufuss E., 2021a, GCN Circular, 29506
Blaufuss E., 2021b, GCN Circular, 31249
Blaufuss E., Kintscher T., Lu L., Tung C. F., 2019, in 36th International Cosmic Ray Conference (ICRC2019). p. 1021, preprint (arXiv:1908.04884)
Blondin S., Tonry J. L., 2007, ApJ, 666, L1024
Carosi A., et al., 2021, preprint (arXiv:2108.04309)
Chambers K. C., et al., 2016, preprint (arXiv:1612.05560)
Cherenkov Telescope Array Consortium, et al., 2019, Science with the Cherenkov Telescope Array,
Dekany R., et al., 2020, PASP, 132, 038001
Evans P. A., et al., 2015, MNRAS, 448, 2210
Farrar G. R., Gruzinov A., 2009, ApJ, 693, L329
Ferrigno C., et al., 2021, New A Rev., 92, 101595
Flesch E. W., 2021, preprint (arXiv:2105.12985)
Franckowiak A., et al., 2020, ApJ, 893, L162
Fremling C., et al., 2020, ApJ, 895, L32
Frostig D., et al., 2020, in Society of Photo-Optical Instrumentation Engineers (SPIE) Conference Series. p. 1144767, preprint (arXiv:2105.01219),
Gaia Collaboration, et al., 2018, A&A, 616, 1
Galama T. J., et al., 1998, Nature, 395, 670
Garrappa S., Buson S., Franckowiak A., Giroletti M., Liodakis I., Nanci C., 2021, PoS, ICRC2021, 956
Ginsburg A., et al., 2019, AJ, 157, 98
Giommi P., Glauch T., Padovani P., Resconi E., Turcati A., Chang Y. L., 2020a, MNRAS, 497, 865
Giommi P., Padovani P., Oikonomou F., Glauch T., Paiano S., Resconi E., 2020b, A&A, 640, 4
Giommi P., Glauch T., Resconi E., 2020c, ATel, 13394, 1
Graham M. J., et al., 2019, PASP, 131, 078001
Guillochon J., Nicholl M., Villar V. A., Mockler B., Narayan G., Mandel K. S., Berger E., Williams P. K. G., 2018, ApJS, 236, 6
Hayasaki K., 2021, Nature Astron., 5, 436
Helou G., Madore B. F., Schmitz M., Bicay M. D., Wu X., Bennett J., 1991, in Albrecht M. A., Egret D.eds, Astrophysics and Space Science Library Vol. 171, Data bases and On-line Data in Astronomy. p. 89, Springer, The Netherlands
Holmbo S., et al., 2019, ATel, 12661, 1
IceCube Collaboration, 2013, Science, 342, 1242856
IceCube Collaboration, et al., 2018, Science, 361, eaat1378
Ivezić Ž., et al., 2019, ApJ, 873, L111
Kadler M., et al., 2021, preprint (arXiv:2108.00383)
Kasliwal M. M., et al., 2020, ApJ, 905, L145
Kiehlmann S., Hovatta T., Kadler M., Max-Moerbeck W., Readhead A. C. S., 2019, ATel, 12996, 1
Kopper C., 2018, GCN Circular, 22669
Kopper C., 2019a, GCN Circular, 23605
Kopper C., 2019b, GCN Circular, 24028

Kopper C., 2019c, GCN Circular, 24392
Kowalski M., Mohr A., 2007, Astropart. Phys., 27, 533
Krauss F., Gregoire T., Fox D. B., Kennea J., Evans P., 2020, ATel, 13395, 1
Lagunas Gualda C., 2020a, GCN Circular, 26802
Lagunas Gualda C., 2020b, GCN Circular, 26832
Lagunas Gualda C., 2020c, GCN Circular, 27719
Lagunas Gualda C., 2020d, GCN Circular, 27950
Lagunas Gualda C., 2020e, GCN Circular, 28411
Lagunas Gualda C., 2020f, GCN Circular, 28468
Lagunas Gualda C., 2020g, GCN Circular, 28504
Lagunas Gualda C., 2020h, GCN Circular, 28532
Lagunas Gualda C., 2020i, GCN Circular, 28715
Lagunas Gualda C., 2020j, GCN Circular, 28889
Lagunas Gualda C., 2020k, GCN Circular, 28927
Lagunas Gualda C., 2020l, GCN Circular, 28969
Lagunas Gualda C., 2020m, GCN Circular, 29012
Lagunas Gualda C., 2021a, GCN Circular, 29454
Lagunas Gualda C., 2021b, GCN Circular, 30153
Lagunas Gualda C., 2021c, GCN Circular, 30468
Lagunas Gualda C., 2021d, GCN Circular, 31085
Lagunas Gualda C., 2021e, GCN Circular, 31126
Lagunas Gualda C., et al., 2021, PoS, ICRC2021, 1045
Lien A., Sakamoto T., Gehrels N., Palmer D. M., Barthelmy S. D., Graziani C., Cannizzo J. K., 2014, ApJ, 783, L24
Lincetto M., 2021a, GCN Circular, 30862
Lincetto M., 2021b, GCN Circular, 30957
Lincetto M., 2021c, GCN Circular, 31241
Lourie N. P., et al., 2020, in Society of Photo-Optical Instrumentation Engineers (SPIE) Conference Series. p. 114479K, preprint (arXiv:2102.01109),
Lucarelli F., et al., 2019, ApJ, 870, L136
Lyman J. D., Bersier D., James P. A., Mazzali P. A., Eldridge J. J., Fraser M., Pian E., 2016, MNRAS, 457, 328
Mannheim K., 1993, A&A, 269, 67
Marcotulli L., Di Mauro M., Ajello M., 2020, ApJ, 896, L6
Masci F. J., et al., 2019, PASP, 131, 018003
Morgan R., et al., 2019, ApJ, 883, L125
Murase K., 2007, Phys. Rev. D, 76, 123001
Murase K., Thompson T. A., Lacki B. C., Beacom J. F., 2011, Phys. Rev. D, 84, 043003
Nakar E., 2015, ApJ, 807, L172
Necker J., Stein R., Weimann S., Reusch S., Franckowiak A., 2021, GCN Circular, 30349
Necker J., et al., 2022, MNRAS, 516, 2455
Nordin J., et al., 2019, A&A, 631, 147
Oikonomou F., Petropoulou M., Murase K., Tohuvavohu A., Vasilopoulos G., Buson S., Santander M., 2021, J. Cosmology Astropart. Phys., 2021, 082
Oke J. B., et al., 1995, PASP, 107, 375
Padovani P., Resconi E., Giommi P., Arsioli B., Chang Y. L., 2016, MNRAS, 457, 3582
Padovani P., Giommi P., Resconi E., Glauch T., Arsioli B., Sahakyan N., Huber M., 2018, MNRAS, 480, 192
Paliya V. S., Böttcher M., Olmo-García A., Domínguez A., Gil de Paz A., Franckowiak A., Garrappa S., Stein R., 2020, ApJ, 902, L29
Pan-Starrs Collaboration, et al., 2019, A&A, 626, 117
Pastorello A., et al., 2006, MNRAS, 370, 1752
Patterson M. T., et al., 2019, PASP, 131, 018001
Perley D. A., et al., 2020, ApJ, 904, L35
Petropoulou M., Oikonomou F., Mastichiadis A., Murase K., Padovani P., Vasilopoulos G., Giommi P., 2020, ApJ, 899, L113
Pitik T., Tamborra I., Angus C. R., Auchettl K., 2022, ApJ, 929, L163
Plavin A., Kovalev Y. Y., Kovalev Y. A., Troitsky S., 2020, ApJ, 894, L101
Plavin A. V., Kovalev Y. Y., Kovalev Y. A., Troitsky S. V., 2021, ApJ, 908, L157
Reguitti A., et al., 2019, ATel, 13133, 1
Reusch S., 2020, simeonreusch/ztffps: Release (3), https://doi.org/10.5281/zenodo.4049711
Reusch S., Stein R., 2020a, GCN Circular, 26747
Reusch S., Stein R., 2020b, GCN Circular, 26813
Reusch S., Stein R., 2020c, GCN Circular, 26816
Reusch S., Stein R., Franckowiak A., 2020a, GCN Circular, 27721
Reusch S., Stein R., Franckowiak A., Gezari S., 2020b, GCN Circular, 27872
Reusch S., Stein R., Franckowiak A., Sollerman J., Schweyer T., Barbarino C., 2020c, GCN Circular, 27910
Reusch S., Stein R., Franckowiak A., Necker J., Sollerman J., Barbarino C., Schweyer T., 2020d, GCN Circular, 27980
Reusch S., Stein R., Franckowiack A., 2020e, GCN Circular, 28005
Reusch S., Stein R., Franckowiak A., Andreoni I., Coughlin M., 2020f, GCN Circular, 28441
Reusch S., Stein R., Franckowiak A., Schulze S., Sollerman J., 2020g, GCN Circular, 28465
Reusch S., Stein R., Weimann S., Franckowiak A., 2020h, GCN Circular, 28520
Reusch S., Weimann S., Stein R., Franckowiak A., 2020i, GCN Circular, 28609
Reusch S., Weimann S., Stein R., Franckowiak A., 2020j, GCN Circular, 29031
Reusch S., Weimann S., Stein R., Coughlin M., Franckowiak A., 2021, GCN Circular, 29461
Reusch S., et al., 2022, Phys. Rev. Lett., 128, 221101
Rodrigues X., Garrappa S., Gao S., Paliya V. S., Franckowiak A., Winter W., 2021, ApJ, 912, L54
Sagiv I., et al., 2014, AJ, 147, 79
Santander M., 2019a, GCN Circular, 24981
Santander M., 2019b, GCN Circular, 25402
Santander M., 2019c, GCN Circular, 26620
Santander M., 2020a, GCN Circular, 27651
Santander M., 2020b, GCN Circular, 27997
Santander M., 2020c, GCN Circular, 28575
Santander M., 2021a, GCN Circular, 29688
Santander M., 2021b, GCN Circular, 29951
Santander M., 2021c, GCN Circular, 29976
Santander M., 2021d, GCN Circular, 30026
Santander M., 2021e, GCN Circular, 30056
Santander M., 2021f, GCN Circular, 30342
Santander M., 2021g, GCN Circular, 30559
Santander M., 2021h, GCN Circular, 30627
Santander M., 2021i, GCN Circular, 31093
Santander M., 2021j, GCN Circular, 31110
Santander M., 2021k, GCN Circular, 31195
Satalecka K., Bernardini E., Dorner D., Kukec Mezek G., Jin W., 2021, preprint (arXiv:2109.04350)
Senno N., Murase K., Mészáros P., 2016, Phys. Rev. D, 93, 083003
Stein R., 2019a, GCN Circular, 25225
Stein R., 2019b, GCN Circular, 25802
Stein R., 2019c, GCN Circular, 25913
Stein R., 2019d, GCN Circular, 26341
Stein R., 2019e, GCN Circular, 26435
Stein R., 2020a, GCN Circular, 26655
Stein R., 2020b, GCN Circular, 26696
Stein R., 2020c, GCN Circular, 27235
Stein R., 2020d, GCN Circular, 27534
Stein R., 2020e, GCN Circular, 27865
Stein R., 2020f, GCN Circular, 28210
Stein R., Reusch S., 2020, GCN Circular, 26667
Stein R., et al., 2019a, ATel, 12730, 1
Stein R., et al., 2019b, ATel, 12879, 1
Stein R., Franckowiak A., Kasliwal M. M., Andreoni I., Coughlin M., Singer L. P., Masci F., van Velzen S., 2019c, ATel, 12974, 1
Stein R., Franckowiak A., Kowalski M., Kasliwal M., 2019d, GCN Circular, 25824
Stein R., Franckowiak A., Necker J., Gezari S., van Velzen S., 2019e, GCN Circular, 25929
Stein R., Necker J., Bradascio F., simonegarrappa, 2020a, icecube/flarestack, https://doi.org/10.5281/zenodo.3619383
Stein R., Reusch S., Weimann S., Coughlin M., 2020b, GCN Circular, 28757

Stein R., Weimann S., Reusch S., Franckowiak A., 2020c, GCN Circular, 29172
Stein R., Reusch S., Necker J., 2021a, desy-multimessenger/nuztf: v2.1.0 Release, https://doi.org/10.5281/zenodo.5217976
Stein R., et al., 2021b, Nature Astron., 5, 510
Stein R., Weimann S., Necker J., Reusch S., Franckowiak A., Zwicky Transient Facility, Growth Collaboration, 2021c, GCN Circular, 29999
Stein R., Weimann S., Reusch S., Necker J., Franckowiak A., Coughlin M., Zwicky Transient Facility collaboration, Global Relay of Observatories Watching Transients Happen Collaboration, 2021d, GCN Circular, 30644
Stern D., et al., 2012, ApJ, 753, L30
Stoughton C., et al., 2002, AJ, 123, 485
Strolger L.-G., et al., 2015, ApJ, 813, L93
Strotjohann N. L., Kowalski M., Franckowiak A., 2019, A&A, 622, 9
Taboada I., 2018, GCN Circular, 23338
Taboada I., 2019, GCN Circular, 23918
Taubenberger S., et al., 2006, MNRAS, 371, 1459
van Velzen S., et al., 2021, ApJ, 908, L4
Waxman E., Bahcall J., 1997, Phys. Rev. Lett., 78, 2292
Weimann S., Stein R., Reusch S., Franckowiak A., 2020a, GCN Circular, 28551
Weimann S., Stein R., Reusch S., Franckowiak A., 2020b, GCN Circular, 28989
Weimann S., Reusch S., Necker J., Stein R., Franckowiak A., Zwicky Transient Facility, Growth Collaboration, 2021, GCN Circular, 30870
Wright E. L., et al., 2010, AJ, 140, 1868

APPENDIX A: NOT FOLLOWED UP

Those alerts not observed by ZTF are summarized in Table A1. Of those 57 alerts not followed up, the primary reasons were proximity to the Sun (18/55), alerts with poor localization and low astrophysical probability (16/55) and alert retraction (10/55). The full breakdown of neutrino observations statistics can be seen in Fig. A1.

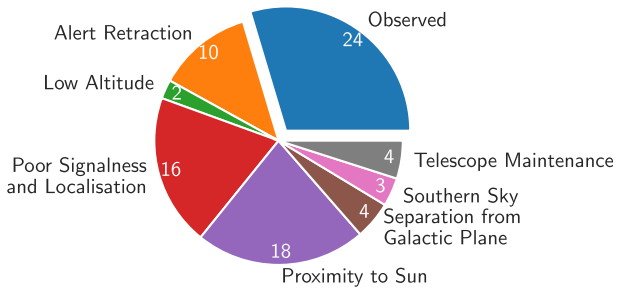

Figure A1. Breakdown of the neutrino follow-up programme, as of 2021 December 31.

Table A1. Summary of the 57 neutrino alerts that were not followed up by ZTF since survey start on 2018 March 20.

Cause	Events
Alert retraction	IC180423A (Kopper 2018) IC181031A (Blaufuss 2018c) IC190205A (Blaufuss 2019b) IC190529A (Blaufuss 2019d) IC200120A (Lagunas Gualda 2020b) IC200728A (Blaufuss 2020d) IC201115B (Blaufuss 2020i) IC210213A (Blaufuss 2021a) IC210322A (Santander 2021a) IC210519A (Santander 2021e)
Proximity to sun	IC180908A (Blaufuss 2018a) IC181014A (Taboada 2018) IC190124A (Blaufuss 2019a) IC190704A (Santander 2019a) IC190712A (Blaufuss 2019g) IC190819A (Santander 2019b) IC191119A (Blaufuss 2019i) IC200227A (Stein 2020c) IC200421A (Blaufuss 2020a) IC200615A (Lagunas Gualda 2020d) IC200806A (Stein 2020f) IC200921A (Lagunas Gualda 2020f) IC200926B (Blaufuss 2020f) IC201014A (Blaufuss 2020g) IC201115A (Lagunas Gualda 2020j) IC201221A (Blaufuss 2020j) IC211117A (Santander 2021i) IC211123A (Santander 2021j)
Low altitude	IC191215A (Stein 2019e) IC211023A (Lincetto 2021b)
Southern sky	IC190104A (Kopper 2019a) IC190331A (Kopper 2019b) IC190504A (Kopper 2019c)
Separation from galactic plane	IC201114A (Blaufuss 2020h) IC201120A (Lagunas Gualda 2020k) IC210516A (Santander 2021d) IC210730A (Santander 2021g)
Poor signalness and localization	IC190221A (Taboada 2019) IC190629A (Blaufuss 2019f) IC190922A (Stein 2019b) IC191122A (Blaufuss 2019j) IC191204A (Stein 2019d) IC191231A (Santander 2019c) IC200410A (Stein 2020d) IC200425A (Santander 2020a) IC200523A (Blaufuss 2020b) IC200614A (Blaufuss 2020c) IC200911A (Lagunas Gualda 2020e) IC210503A (Santander 2021b) IC210608A (Lagunas Gualda 2021b) IC210717A (Lagunas Gualda 2021c) IC211125A (Lagunas Gualda 2021e) IC211216A (Lincetto 2021c)
Telescope maintenance	IC181023A (Blaufuss 2018b) IC211116A (Lagunas Gualda 2021d) IC211208A (Santander 2021k) IC211216B (Blaufuss 2021b)

APPENDIX B: CANDIDATES

Candidates from each neutrino follow-up programme are listed in tables B1 – B20. Those candidates mentioned in the main text are highlighted in bold. For four neutrino campaigns (IC200107A, IC201007A, IC201222A, and IC210922A), no candidates were identified, and there are no corresponding lists.

Table B1. Candidates for IC190503A.

ZTF name	IAU name	Classification	Peak magnitude
ZTF19aatqcwq	–	AGN variability	20.6 (g)
ZTF19aatqlwq	–	AGN variability	21.2 (r)

Table B2. Candidates for IC190619A.

ZTF name	IAU name	Classification	Peak magnitude
ZTF18abolwbb	–	AGN variability	19.4 (r)
ZTF18abueqkl	AT 2020kqj	AGN variability	19.3 (g)
ZTF18acehkni	–	AGN variability	19.4 (r)
ZTF18actxchc	–	AGN variability	18.0 (g)
ZTF19aadaszg	SN 2019rg	SN Ia	15.9 (r)
ZTF19aawnawu	–	AGN variability	20.0 (g)
ZTF19aaycone	–	AGN variability	17.9 (g)
ZTF19aaycool	–	AGN variability	20.3 (g)
ZTF19aaycosc	–	AGN variability	19.3 (r)
ZTF19aaycoxd	–	AGN variability	20.3 (g)
ZTF19abahiwr	AT 2019izf	Unclassified	19.5 (r)
ZTF19abahiya	–	Unclassified	19.6 (r)
ZTF19abahizn	–	AGN variability	19.7 (g)
ZTF19abahjcp	–	AGN variability	20.2 (g)
ZTF19abahlep	–	Unclassified	20.8 (r)
ZTF19abahlka	–	AGN variability	19.8 (i)
ZTF19abajnby	–	AGN variability	20.0 (r)

Table B3. Candidates for IC190730A.

ZTF name	IAU name	Classification	Peak magnitude
ZTF19aanlzzk	–	Artefact	13.8 (g)

Table B4. Candidates for IC190922B.

ZTF name	IAU name	Classification	Peak magnitude
ZTF18acekfly	AT 2019kkd	AGN variability	18.5 (r)
ZTF19abcejyp	AT 2019kkp	AGN variability	19.3 (r)
ZTF19abxtupj	SN 2019pqh	SN II/IIb	20.3 (r)

Table B5. Candidates for IC191001A.

ZTF name	IAU name	Classification	Peak magnitude
ZTF18ablvxkp	–	AGN variability	19.3 (r)
ZTF18absoqfm	–	AGN variability	19.0 (g)
ZTF19aapreis	AT 2019dsg	TDE	17.8 (g)
ZTF19abassjx	–	AGN variability	19.4 (i)
ZTF19abcdynm	–	AGN variability	20.5 (g)
ZTF19abexshr	–	AGN variability	20.2 (r)
ZTF19abjfikj	–	AGN variability	20.9 (g)
ZTF19abjflnc	–	AGN variability	19.2 (i)
ZTF19abjflrg	–	AGN variability	21.3 (g)
ZTF19abjfmem	–	AGN variability	21.5 (g)
ZTF19abwaurq	–	Unclassified	19.5 (r)
ZTF19abzkexb	SN 2019qhl	SN Ia	18.9 (g)
ZTF19acbpqfn	AT 2019rsj	Unclassified	20.4 (g)
ZTF19acbpqui	–	Unclassified	20.5 (g)
ZTF19acbwpqs	–	AGN variability	19.9 (g)
ZTF19acbxahc	–	Unclassified	21.1 (g)
ZTF19acbxanz	–	Unclassified	20.6 (r)
ZTF19acbxaqj	–	Unclassified	20.5 (r)
ZTF19acbxauk	–	Unclassified	20.8 (g)
ZTF19acbxbjq	AT 2019rsk	Unclassified	20.3 (g)
ZTF19accnqlc	–	Unclassified	20.2 (r)

Table B6. Candidates for IC200109A.

ZTF name	IAU name	Classification	Peak magnitude
ZTF18aaidhnq	–	AGN variability	18.1 (r)
ZTF18aceykyg	–	AGN variability	19.0 (g)
ZTF18adgvgdk	–	AGN variability	19.3 (g)
ZTF19aangwsm	–	Artefact	19.8 (g)
ZTF19aapsgtb	–	AGN variability	18.8 (r)
ZTF19aarohku	–	AGN variability	19.8 (r)
ZTF19acmwlds	AT 2019yfm	Unclassified	19.7 (g)
ZTF19adcdxgc	–	AGN variability	19.6 (g)
ZTF20aaeunmm	–	AGN variability	20.4 (g)
ZTF20aaeuufe	AT 2019yii	Unclassified	20.4 (r)
ZTF20aaevfrv	–	Star	20.7 (g)
ZTF20aaevfth	AT 2020ux	Unclassified	21.2 (g)
ZTF20aaevfwa	AT 2019zxa	Unclassified	20.6 (r)
ZTF20aaevgvt	AT 2020uw	Artefact	20.5 (r)
ZTF20aagvvve	–	Artefact	19.7 (r)
ZTF20aagvvvh	–	Artefact	19.8 (r)
ZTF20aagvvvk	–	Artefact	19.9 (r)
ZTF20aagvvvn	–	Artefact	20.0 (r)
ZTF20aagwcup	AT 2020dtc	Artefact	19.9 (r)
ZTF20aagwcuq	–	Unclassified	20.0 (r)
ZTF20aagwcuu	–	Unclassified	20.0 (r)
ZTF20aagwcuv	–	Unclassified	19.9 (r)
ZTF20aagxfta	–	Unclassified	19.9 (g)

Table B7. Candidates for IC200117A.

ZTF name	IAU name	Classification	Peak magnitude
ZTF19acxopgh	AT 2019zyu	Unclassified	19.4 (r)
ZTF19adceqeb	–	AGN variability	19.6 (g)
ZTF20aacztcp	AT 2020ko	AGN variability	19.0 (r)
ZTF20aaglixd	AT 2020agt	Unclassified	21.2 (g)

Table B8. Candidates for IC200512A.

ZTF name	IAU name	Classification	Peak magnitude
ZTF18aazvbyj	–	Star	17.5 (r)
ZTF18abjnqos	–	Star	12.9 (r)
ZTF18abmfxbh	–	Artefact	17.5 (r)
ZTF18abmfzmm	–	Artefact	17.1 (r)
ZTF19acgpzgi	–	Artefact	15.5 (g)
ZTF20aazqsfe	–	Star	19.6 (g)

Table B9. Candidates for IC200530A.

ZTF name	IAU name	Classification	Peak magnitude
ZTF18aaimsgg	AT 2018lnq	Artefact	16.6 (r)
ZTF18aamjqes	AT 2020llg	AGN variability	16.9 (r)
ZTF18aaneyxs	–	Artefact	14.6 (r)
ZTF18aavecmo	AT 2020llh	AGN flare	19.6 (i)
ZTF18aazkjyd	–	Artefact	14.7 (r)
ZTF18abrwqpr	AT 2020lli	AGN flare	19.6 (g)
ZTF19aaonfhr	AT 2020llj	AGN variability	20.4 (r)
ZTF19aascfca	–	AGN variability	20.7 (g)
ZTF19aascffj	–	AGN variability	20.0 (g)
ZTF19aatubsj	AT 2019fdr	TDE	17.9 (i)
ZTF19abregmj	AT 2020llk	AGN variability	19.9 (g)
ZTF20aaifyfd	AT 2020lll	AGN variability	19.9 (g)
ZTF20aaifyrs	SN 2020awa	SN Ia	17.0 (r)
ZTF20aarbktd	SN 2020djn	SN II	18.0 (i)
ZTF20aavnpug	AT 2020idu	Dwarf nova	15.9 (i)
ZTF20aawyens	AT 2020lpp	AGN variability	19.7 (i)
ZTF20aaxcdok	AT 2020lpq	Unclassified	20.1 (r)
ZTF20aaxyglx	AT 2020llm	AGN variability	20.3 (g)
ZTF20abaofgz	AT 2020lpr	AGN variability	19.9 (r)
ZTF20abbpkpa	SN 2020lam	SN II	18.8 (g)
ZTF20abcnrcb	–	AGN variability	19.3 (g)
ZTF20abdnovz	–	Star	21.3 (r)
ZTF20abdnowa	AT 2020lln	Artefact	20.7 (g)
ZTF20abdnowp	AT 2020llo	Unclassified	21.1 (g)
ZTF20abdnowx	–	AGN variability	21.3 (g)
ZTF20abdnoxe	–	AGN variability	20.3 (g)
ZTF20abdnoxm	AT 2020llp	Unclassified	20.8 (g)
ZTF20abdnoyu	AT 2020lps	Unclassified	21.4 (g)
ZTF20abdnozk	AT 2020llq	AGN variability	20.6 (r)
ZTF20abdnpae	AT 2020lpt	Unclassified	20.9 (g)
ZTF20abdnpbp	AT 2020llr	AGN variability	20.7 (r)
ZTF20abdnpbq	AT 2020lpw	AGN variability	21.0 (r)
ZTF20abdnpbu	AT 2020lpx	Unclassified	21.0 (g)
ZTF20abdnpdo	SN 2020lls	SN Ic	19.0 (r)
ZTF20abdqzjl	–	Star	20.4 (r)
ZTF20abdqzjr	–	AGN variability	21.1 (r)
ZTF20abdqzkq	AT 2020lpu	Star	20.7 (g)
ZTF20abdqzkr	–	AGN variability	21.1 (g)
ZTF20abdrnjw	–	Star	21.3 (r)
ZTF20abdrnlg	AT 2020lpv	Unclassified	20.9 (r)
ZTF20abdrnmp	–	AGN variability	21.6 (r)

Table B10. Candidates for IC200620A.

ZTF name	IAU name	Classification	Peak magnitude
ZTF18acvhwtf	AT 2020ncs	AGN variability	19.7 (r)
ZTF20abgvabi	AT 2020ncr	AGN variability	20.2 (r)

Table B11. Candidates for IC200916A.

ZTF name	IAU name	Classification	Peak magnitude
ZTF18acccxxf	AT 2020tnn	AGN variability	19.7 (g)
ZTF18adbbnry	AT 2020tnn	AGN variability	19.8 (g)
ZTF20acaapwk	SN 2020tno	SN Ia	18.9 (r)
ZTF20acaapwn	–	Unclassified	21.0 (g)
ZTF20acaapwo	AT 2020tnp	Unclassified	20.4 (r)
ZTF20acayuno	–	AGN variability	21.1 (r)

Table B12. Candidates for IC200926A.

ZTF name	IAU name	Classification	Peak magnitude
ZTF18achvmdz	–	AGN variability	18.9 (i)
ZTF18acwfrle	–	Star	15.4 (g)

Table B13. Candidates for IC200929A.

ZTF name	IAU name	Classification	Peak magnitude
ZTF20aamoxyt	–	AGN flare	19.8 (g)

Table B14. Candidates for IC201021A.

ZTF name	IAU name	Classification	Peak magnitude
ZTF18abmkdiy	AT 2019cvb	AGN variability	18.7 (i)
ZTF20abfaado	AT 2020nbr	Star	19.3 (i)
ZTF20acinqzo	–	AGN variability	19.6 (i)
ZTF20acmxnpa	AT 2020ybb	Unclassified	20.6 (g)

Table B15. Candidates for IC201130A.

ZTF name	IAU name	Classification	Peak magnitude
ZTF17aadmvpm	–	Artefact	16.1 (g)
ZTF18abxrpgu	AT 2021ury	AGN flare	18.8 (r)
ZTF18achpvrl	–	AGN variability	19.1 (r)
ZTF19aaagxcv	–	AGN variability	18.4 (g)
ZTF20aceidvg	–	AGN variability	19.7 (g)
ZTF20acmnnwf	–	AGN variability	19.9 (r)
ZTF20acuqdeu	AT 2020aehs	Unclassified	19.8 (g)
ZTF20acxbkpz	–	Unclassified	20.5 (r)

Table B16. Candidates for IC201209A.

ZTF name	IAU name	Classification	Peak magnitude
ZTF18abwhosy	–	AGN variability	19.3 (r)
ZTF20abvxjup	–	AGN variability	20.0 (g)
ZTF20acycunv	SN 2020addp	SN IIP	19.4 (r)

Table B17. Candidates for IC210210A.

ZTF name	IAU name	Classification	Peak magnitude
ZTF19aaapmca	–	AGN variability	18.6 (r)
ZTF19aailrrn	–	AGN variability	20.0 (g)
ZTF19aasfvho	–	AGN variability	19.4 (g)
ZTF19aasfvqm	–	AGN flare	18.2 (r)
ZTF20aadynqa	–	AGN variability	20.1 (g)
ZTF20aajcpde	–	AGN variability	19.5 (g)
ZTF21aafmkun	–	AGN variability	19.4 (r)
ZTF21aajxjmv	–	Star	21.3 (r)
ZTF21aajxjmy	–	Star	21.1 (g)
ZTF21aajxjnb	–	AGN variability	22.1 (g)
ZTF21aajxjnc	–	AGN variability	21.7 (g)
ZTF21aajxjrn	–	AGN variability	20.1 (r)
ZTF21aajxjrv	AT 2021clu	Unclassified	20.9 (r)
ZTF21aajxjry	AT 2021clv	Unclassified	21.5 (r)
ZTF21aajxjsa	–	AGN variability	21.7 (r)
ZTF21aajxkls	–	AGN variability	21.1 (g)
ZTF21aakiqpj	–	Star	22.1 (g)

Table B18. Candidates for IC210510A.

ZTF name	IAU name	Classification	Peak magnitude
ZTF19aadzayi	–	Star	15.0 (r)
ZTF19aawqcum	–	AGN variability	19.1 (g)
ZTF20abhfiyd	–	Star	19.6 (g)
ZTF20acinvxv	–	Unclassified	21.0 (r)
ZTF20acinwlt	–	AGN variability	21.0 (r)
ZTF21aaiuekm	–	Star	19.5 (g)

Table B19. Candidates for IC210629A.

ZTF name	IAU name	Classification	Peak magnitude
ZTF18abteipt	AT 2019gnu	AGN variability	17.1 (r)
ZTF21abecljv	AT 2021osi	AGN variability	19.8 (i)
ZTF21abllruf	–	Artefact	17.5 (i)

Table B20. Candidates for IC210811A.

ZTF name	IAU name	Classification	Peak magnitude
ZTF20abjezpo	–	Star	19.7 (r)
ZTF21absmcwm	–	AGN variability	20.8 (g)

[1]*Deutsches Elektronen-Synchrotron (DESY), Platanenallee 6, D-15378 Zeuthen, Germany*
[2]*Institut fur Physik, Humboldt-Universität zu Berlin, D-12489 Berlin, Germany*
[3]*Division of Physics, Mathematics and Astronomy, California Institute of Technology, Pasadena, CA 91125, USA*
[4]*Fakultät für Physik & Astronomie, Ruhr-Universität Bochum, D-44780 Bochum, Germany*
[5]*Oskar Klein Centre, Department of Astronomy, Stockholm University, 10691 Stockholm, Sweden*
[6]*Department of Astronomy, University of Maryland, College Park, MD 20742, USA*
[7]*Astrophysics Science Division, NASA Goddard Space Flight Center, Mail Code 661, Greenbelt, MD 20771, USA*
[8]*Max Planck Institute for Extraterrestrial Physics, 85748 Garching bei München, Germany*
[9]*Institute of Applied Mathematics, Academy of Mathematics and Systems Science, Beijing 100190, China*
[10]*Kavli Institute for Astronomy and Astrophysics, Beijing 100084, China*
[11]*Joint Space-Science Institute, University of Maryland, College Park, MD 20742, USA*
[12]*Department of Astronomy, University of Maryland, College Park, MD 20742, USA*
[13]*Astrophysics Science Division, NASA Goddard Space Flight Center, Mail Code 661, Greenbelt, MD 20771, USA*
[14]*Department of Astronomy, DIRAC Institute, University of Washington, 3910 15th Avenue NE, Seattle, WA 98195, USA*
[15]*Department of Astronomy, University of California, Berkeley, CA 94720, USA*
[16]*Lawrence Berkeley National Laboratory, 1 Cyclotron Road, MS 50B-4206, Berkeley, CA 94720, USA*
[17]*School of Physics and Astronomy, University of Minnesota, Minneapolis, MN 55455, USA*
[18]*MIT-Kavli Institute for Astrophysics and Space Research, 77 Massachusetts Avenue, Cambridge, MA 02139, USA*
[19]*Space Telescope Science Institute, 3700 San Martin Dr, Baltimore, MD 21218, USA*
[20]*IPAC, California Institute of Technology, 1200 E. California, CA 91125, USA*
[21]*Center for Gravitation, Cosmology and Astrophysics, Department of Physics, University of Wisconsin–Milwaukee, Milwaukee, WI 53201, USA*
[22]*Institute of Astronomy, National Tsing Hua University, Hsinchu 30013, Taiwan*
[23]*Center for Data Driven Discovery, California Institute of Technology, Pasadena, CA 91125, USA*
[24]*Physics Department, University of Wisconsin–Madison, Madison, WI 53706, USA*
[25]*Caltech Optical Observatories, California Institute of Technology, Pasadena, CA 91125, USA*
[26]*Leiden Observatory, Leiden University, Postbus 9513, 2300 RA, Leiden, The Netherlands*

This paper has been typeset from a TEX/LATEX file prepared by the author.